PROCEEDINGS A

royalsocietypublishing.org/journal/rspa

Perspective

Cite this article: Bažant ZP. 2019 Design of quasibrittle materials and structures to optimize strength and scaling at probability tail: an apercu. *Proc. R. Soc. A* **475**: 20180617. http://dx.doi.org/10.1098/rspa.2018.0617

Received: 25 September 2018
Accepted: 27 February 2019

Subject Areas:
materials science

Keywords:
size effect, scaling, quasibrittle fracture, material randomness, failure probability, stength distribution, interatomic bond failure, activation energy, Weibull distribution, weakest link chain

Author for correspondence:
Zdeněk P. Bažant
e-mail: z-bazant@northwestern.edu

Design of quasibrittle materials and structures to optimize strength and scaling at probability tail: an apercu

Zdeněk P. Bažant

McCormick Institute Professor and W.P. Murphy Professor of Civil and Mechanical Engineering and Materials Science, Northwestern University, 2145 Sheridan Road, CEE/A135, Evanston, IL 60208, USA

The objective in materials or structure design has been to maximize the mean strength. However, as generally agreed, engineering structures, such as bridges, aircraft or microelectromechanical systems must be designed for tail probability of failure less than 10^{-6} per lifetime. But this objective is not the same. Indeed, a quasibrittle material or structure with a superior mean strength can have, for the same coefficient of variation, an inferior strength at the less than 10^{-6} tail. This tail is unreachable by histogram testing. So, one needs a rational theory, physically based and experimentally verified indirectly, which is feasible by size effect. Focusing on the results at the writer's home institution, this inaugural article (written three years *ex post facto*) reviews recent results towards this goal, concerned with quasibrittle materials such as concretes, rocks, tough ceramics, fibre composites, bone and most materials on the micrometer scale. The theory is anchored at the atomic scale because only on that scale the failure probability is known—it is given by the frequency of breakage of bonds, governed by the activation energy barriers in the transition rate theory. An analytical way to scale it up to the macroscale representative volume element (RVE) has been found. Structures obeying the weakest-link model are considered but, for quasibrittle failures, the number of links, each corresponding to one RVE, must be considered as finite. The result is a strength probability distribution transiting from Weibullian to Gaussian, depending on the structure size. The Charles-Evans and Paris laws for subcritical crack growth under static and cyclic fatigue are also derived from the transition-rate theory. This yields a size-dependent Gauss–Weibull distribution of

THE ROYAL SOCIETY PUBLISHING

lifetime. Close agreement with numerous published test data is achieved. Discussed next are new results on materials with a well-defined microscale architecture, particularly biomimetic imbricated (or staggered) lamellar materials, exemplified by nacre, a material of astonishing mean strength compared to its constituents. This architecture is idealized as a diagonally pulled fishnet, which is shown to be amenable to an analytical solution of the strength probability distribution. The solution is verified by million Monte Carlo simulations for each of the fishnets of various shapes and sizes. In addition to the classical weakest-link and the fibre-bundle models, the fishnet is found to be the third strength probability model that is amenable to an analytical solution. The nacreous architecture is shown to provide an additional major (greater than 100%) strengthening at the 10^{-6} failure probability tail. Finally, it is emphasized that the most important consequence of the quasibrittleness, and also the most effective way of calibrating the 10^{-6} tail, is the size effect on the mean structural strength, which permeates all formulations.

1. Introduction

On approach to the centenary of the founding of fracture mechanics in 1921 by Griffith [1], three types of fracture mechanics may be distinguished [2] (figure 1*a*). The first two have become well understood in the past century, while the third is still evolving. These three are:

(1) The linear elastic fracture mechanics (LEFM), in which the crack is considered to be sharp and the entire volume of the structure, which unloads during crack propagation, behaves elastically because the fracture process zone (FPZ) at the crack tip is negligibly small compared to structural dimensions.
(2) The ductile (or cohesive-plastic) fracture mechanics, in which the crack tip is surrounded by a large nonlinear zone that undergoes plastic yielding without softening damage [3]. But the FPZ at the crack tip is still negligibly small, of micrometer dimensions in metals.
(3) The quasibrittle (of cohesive softening) fracture mechanics, which transitions to continuum damage mechanics and damage localization, and is a newer branch of fracture mechanics, whose origin can be traced back to Barenblatt's (1959) idea [4,5] of softening cohesion. Its evolution began in the 1960s [6] and took off seriously in the 1980s [2,7–11]. It represents the limit case of strain localization in continuum damage mechanics treated by nonlocal damage theories [12]. It is characterized by a large, long and wide [2], FPZ, which is approximately of constant size regardless of structure size and shape. The FPZ exhibits progressive material damage in whose surroundings the material is elastic, with virtually no plastic or hardening nonlinear zone in between (the FPZ width in concrete has been evidenced by acoustics, digital image analysis and discrete particle models (e.g. [13–15]).

Aside from Irwin's characteristic length [16], l_0, along the crack line, a second is shared with the ductile cohesive fracture mechanics, and is a consequence of the simultaneous role of fracture energy and material strength, an essential feature is that there exists a second characteristic length, l_1, that is usually dictated by material heterogeneity and which represents the effective width of a propagating FPZ. Due to the finiteness of the FPZ width, the tensorial character of damage in the FPZ matters. In calculations, two versions have been used:

(a) *Cohesive softening* fracture mechanics, in which the width, l_1, of the FPZ is neglected, being shrunken into a line, and the crack opening or slip is modelled by a vectorial stress-displacement relation on the crack extension line, which again allows considering the whole structure volume as elastic and is often tractable analytically.

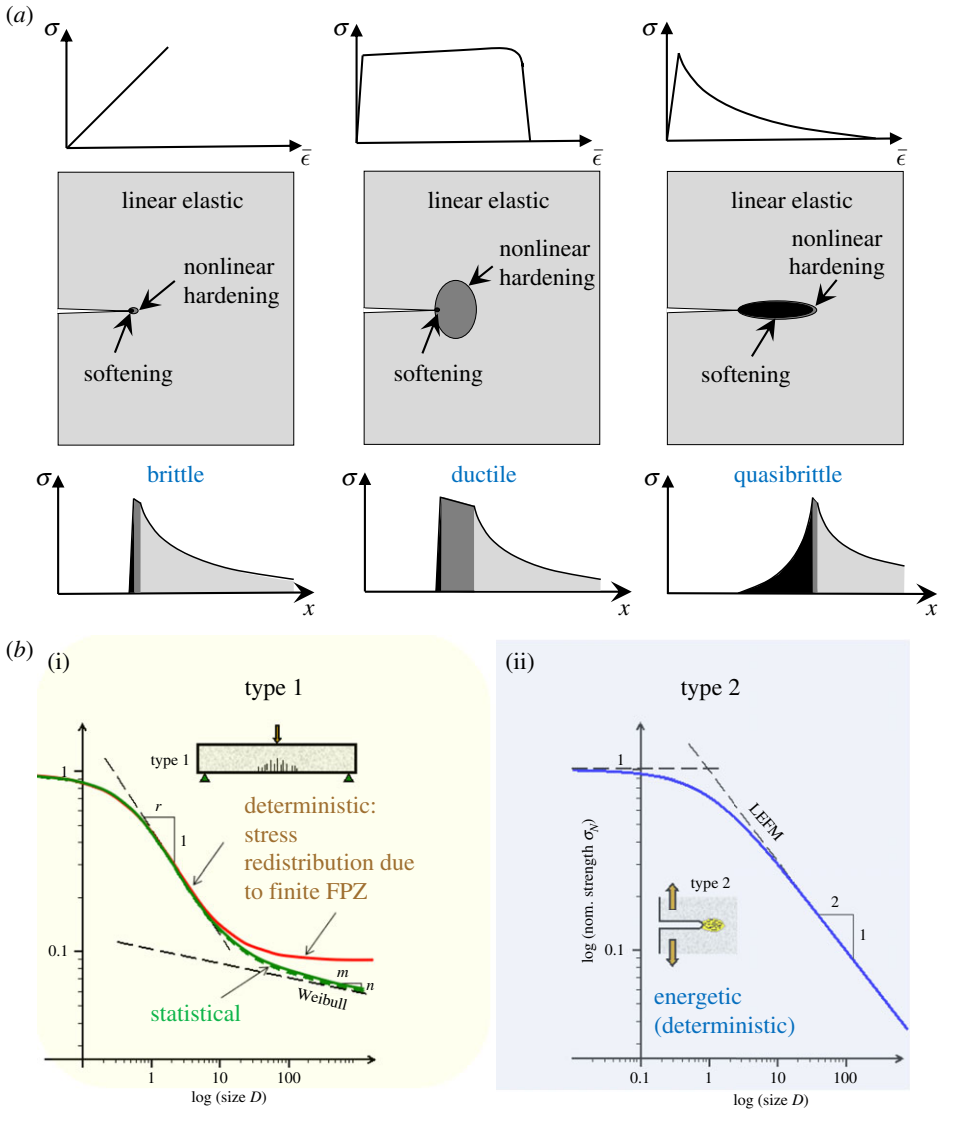

Figure 1. (*a*) Three types of fracture mechanics: brittle, ductile and quasibrittle; (*b*) Two basic types of size effect on the nominal strength of structures, 1–energetic statistical, 2–energetic. (Online version in colour.)

(b) *Quasibrittle* fracture mechanics, in which the finite width, l_1, of the FPZ is taken into account and the FPZ is modelled tensorially [2,10,11]. This is necessary to capture, e.g. the effect of compressive stress parallel to crack plane. This effect is large for quasibrittle materials. It can alone produce splitting fracture but is, unfortunately, lost in the former, simpler, version.

The archetypical quasibrittle material is concrete, which is where the development of quasibrittle fracture mechanics began in the 1970s [2,8,17–19]. Subsequently, it was realized that quasibrittle fracture mechanics, with its size effect, applies to many materials, including tough ceramics, fibre composites, many rocks including shale, stiff clay, bones, sea ice, rigid foams, dental cements, dentine, nacre, biological shells, cartilage, wood, consolidated snow, particle board, paper, carton, cast iron, thin films, carbon nanotubes, fibre-reinforced concrete, cold asphalt

concrete, mortars, masonry, consolidated silt, cemented sand, grouted soil, most refractories and coal.

This inaugural article (written four years *ex post facto*) aims to review the recent advances, with emphasis on the works at the author's home institution, and on the probabilistic safety aspects important for engineering.

(a) Quasibrittleness, heterogeneity and size effect types

The concept of quasibrittleness is relative. It depends on the ratio of structure size to the material inhomogeneity size or, more precisely, to the size of a fully formed FPZ, approximately representing the material characteristic length. All quasibrittle materials become perfectly brittle and follow LEFM on a sufficiently large scale (e.g. concrete on the scale of Hoover Dam), while all brittle materials normally following LEFM become quasibrittle on a sufficiently small scale (e.g. polysilicone on the micrometre scale [20]). The FPZ length in normal strength concrete is about 0.5 m [10], in embrittled polycrystalline metals a few micrometres, for vertical loading of Arctic sea ice about 5 m [21–23]. For in-plane loading of ocean-wide Arctic ice cover (consisting of thick multi-kilometre floes separated by thin ice), it is about 10 km.

The probabilistic quasibrittle strength theory is particularly important for civil engineering, which must deal with materials such as concrete, rocks and soils, notorious for their high random variability, much higher than it is, e.g. for jet engine blades. Yet the probabilistic aspect is equally important for expensive high-tech materials for which extreme reliability is required, as is usually the case in aerospace or nuclear engineering.

The material characteristic length and tensorial nature of quasibrittle fracture govern the localization of distributed damage into distinct fractures whose minimum possible spacing is dictated by material heterogeneity. This localization is a structural phenomenon, governed by the loss of positive definiteness of the second variation of the Helmholtz free energy of a quasibrittle structure in an equilibrium state. The localization is important for, e.g. reinforced concrete, as well as hydraulic fracturing of shale (and is not captured by the popular phase-field model as it currently exists).

In elasticity and plasticity, the scaling of structural strength is trivial—a power law of zero exponent, i.e. stress and strain independence of structure size under geometrically similar scaling. This may explain why the only kind of size effect known prior to 1984 was the Weibull statistical size effect [24]. This size effect is based on the weakest-link chain model (figure 2*a*), in which the number of links has generally been considered infinite. Each link corresponds to one representative volume element (RVE) of the material, which can potentially serve as the fracture-initiating FPZ, provided that the structure has the so-called positive geometry. This is a geometry for which the energy release rate (or the stress intensity factor) increases at constant load as the crack propagates, as is the case for typical fracture test specimens. If the geometry is negative, which is typical of reinforced concrete and is desired for hydraulic cracks in deep shale strata [25], parallel cracks do not localize and grow in a stable manner until the geometry switches to positive.

(b) Types of energetic-statistical size effect

The energetic-statistical size effect is of two types (figure 1*b*). The *Type 1* occurs in structures or specimens with no notch nor preexisting large crack [26–28], provided that the geometry of the structure without a crack is positive [10,29], so that the fracture becomes unstable, i.e. dynamic, as soon as a full FPZ develops, typically at the boundary. The *Type 2* [9,30] occurs when there is either a long enough notch or a preexisting crack that has grown stably at increasing load, provided that the crack or notch length makes the structural geometry positive [10,29]). Type 2 is usually achieved by reinforcement of concrete [10,11,29,31] and also occurs in hydraulic fracturing of deep shale strata [32,33] (one may also discern Type 3 [11,34] but it is very similar to Type 2 and is not discussed here).

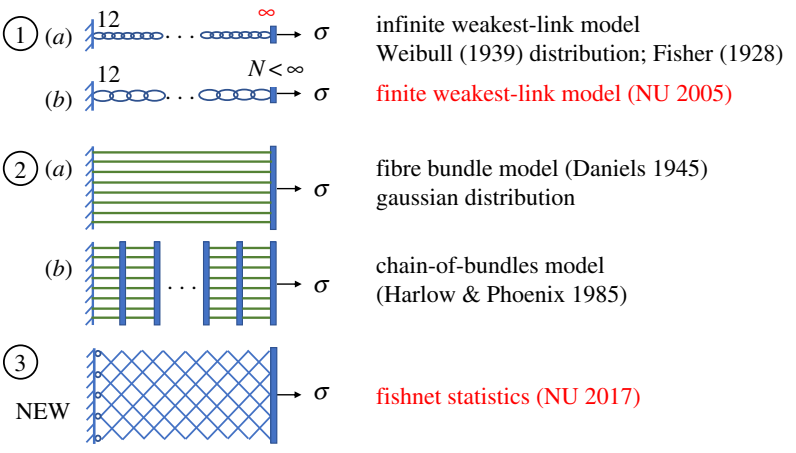

Figure 2. Analytically tractable models of failure probability distribution. (Online version in colour.)

The size effect is usually defined as the effect of structure size on the nominal strength of the geometrically scaled structure, defined as

$$\sigma_N = \frac{P}{A}, \quad A = bD \tag{1.1}$$

σ_N is a load parameter with the dimension of stress and is not necessarily an actual stress at some specific point; P = maximum load (or load capacity) of structure; A, D = characteristic cross-section area and characteristic structure size (measured at homologous locations); and b structure width, constant in the case of two-dimensional scaling. For elastic or elastic-plastic structures governed by a yield criterion, there is no size effect, i.e. σ_N is size independent, which is why σ_N is used to characterize the size effect.

The Type 1 and 2 size effects on the mean strength are quite different (figure 1*b*). In Type 2, the randomness of material strength field affects significantly only the coefficient of variation of structure, but not the mean, and σ_N follows the energetic (deterministic) size effect law [30] (figure 1*b* right):

$$\sigma_N = \sigma_0 \left(1 + \frac{D}{D_0}\right)^{-1/2}, \tag{1.2}$$

where D_0 (transitional size) and σ_0 are constants; D_0 can be expressed in terms of the LEFM solution, if available, and the characteristic length [9,10,15,29,34–36].

In Type 2, the ratio $\beta = D/D_0$ is called the brittleness number of structure. It characterizes brittleness independently of structure geometry [37,38]. Equation (1.2) describes the transition from ductile to brittle structure behaviour as the size increases (note that this fracture mechanics-based concept of brittleness is fundamentally different from the classical concept in materials science, in which the brittle–ductile transition has been regarded purely as a feature of the inelastic stress–strain relation and limit-state envelope of the material [39, Sec. 8.3, 40]), regardless of the energy release and localization aspects of fracture and damage mechanics; see, e.g. [28].

In Type 1, the size effect is mostly deterministic at small sizes and is explained by the fact that FPZ is large enough to cause a significant stress redistribution [29,35,41,42] (figure 1*bi*). The deterministic part has the approximate form $\sigma_N = \sigma_\infty(1 + rD/D_1)^{1/r}$ where σ_∞, D_1 and r are constants. For large sizes, though, the Type 1 size effect becomes dominated by the randomness of the strength field, and the strength distribution converges to Weibullian. The Type 2 converges to Type 1 when the initial crack or notch approaches the FPZ size [43].

This review will be focused mainly on the Type 1 failures, in which the size effect on the mean structural strength has both deterministic and statistical components (for Type 2, see e.g. [10,11]),

the deterministic one being caused by the finiteness of the FPZ size, and the statistical one due to the randomness of the material strength field.

2. Strength distribution and its tail at 10^{-6} failure probability

The sources of risk of structural failure are two: (1) Randomness of material failure or strength, and (2) randomness of loads (including dynamic excitations such as random vibrations or earthquakes). The latter has been extensively studied for decades. But, after Freudenthal's classical study of material flaws [44], the former has been widely neglected. Yet, in the case of quasibrittle structures, the former is a big source of failure risk, which is what we focus on here. The integration of the two sources is well known (e.g. [29,45,46]) and will not be discussed here.

As generally agreed, engineering structures must be designed for failure probability lower than 10^{-6} per lifetime [47–49] (figure 2*a*), which is on the order of magnitude of the risk of death by a falling tree or lightning, and is negligible compared to the risk of death in a car accident (which is about 10^{-2} per lifetime). Typically, only the mean strength and the coefficient of variation are known. But to obtain an accurate extrapolation to the tail at 10^{-6}, the probability distribution of material failure must be known analytically up to that tail, even though the randomness of loads intervenes, too.

Until 2017, there existed only two analytically tractable theories of probability distribution of material or structure strength (1 and 2 in figure 2), and now there are three (3 in figure 2) They are:

(1) The weakest-link model which, for infinite number of links in the chain, leads to the Weibull distribution and applies to perfectly brittle materials (1a in figure 2; figure 3*b*). This distribution was established and experimentally demonstrated by Weibull in 1939 [24]. In mathematics, though, it was discovered by Fisher & Tippett already in 1928 [50]), as one of there and only three possible extreme value distributions (cf. [29,45,46,51,52]).
(2) The fibre-bundle model (2a in figure 2; figure 3*a*,*c*), which applies to ductile (or plastic) structures. Daniels [53] in 1945 proved that if the number of fibres (or parallel elements) tends to infinity, the bundle strength converges to the Gaussian (or normal) distribution regardless of the element properties (but if the elements are brittle many parallel fibres are needed to approach the Gaussian).
(3) the fishnet model (3 in figure 2), which appeared in 2017 and represents the third analytically tractable model [54–56] (figure 3). It will be discussed later.

The Weibull and Gaussian distributions matched to the same mean and coefficient of variation (typically 8% for concrete) are hardly distinguishable (figure 3*a*), and in scattered histograms of less than 300 tests are often indistinguishable. But they differ by almost 2:1 in terms of the distance of the 10^{-6} point from the mean (figure 3*a*). For quasibrittle structures, the strength distributions can be anywhere in between, which translates into enormous uncertainty in the safety factor to be applied.

These observations bring to mind a new question. Why should we strive to maximize the mean material strength?

What matters for structural safety is the strength at the distribution tail with failure probability 10^{-6}. As illustrated in figure 3*c*, its maximization is not an equivalent objective. Depending on the microstructural architecture, a material or structure with an inferior mean strength may have a superior strength in the 10^{-6} tail (figure 3*c*). This tail-mean non-equivalence has been disregarded in materials science and engineering, as well as structural safety assessments. The theory reviewed here shows a remedy.

3. Interatomic bond breakage rate as the basis of failure probability

To capture the 10^{-6} probability, a mathematical model of the strength distribution of quasibrittle material must have a physical basis. For brittle failure, Freudenthal's theory [44] of a critical

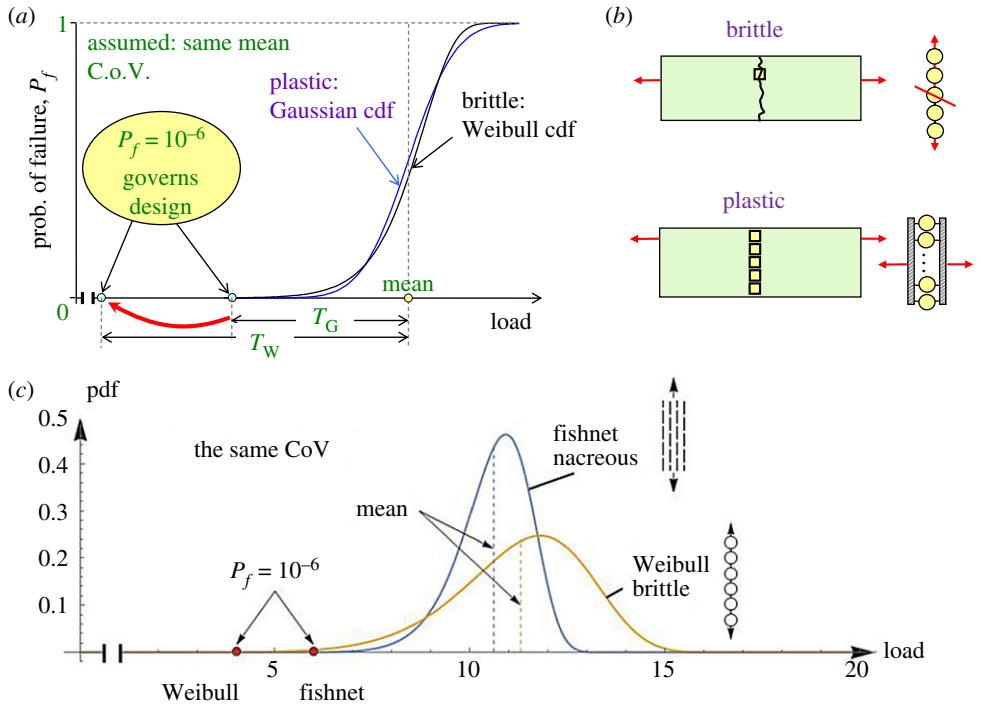

Figure 3. (*a*) Comparison of Gaussian and Weibull distributions for the same mean and same coefficient of variation (CoV = 8%); (*b*) Example of probability density distributions showing that a material with a superior mean strength can have an inferior strength at failure probability 10^{-6}. (Online version in colour.)

material flaw has long been accepted as such a basis. However, this theory amounts to deriving one hypothesis, the Weibull distribution, from a set of three other hypotheses [57,58], namely: (1) the Fréchet distribution of the largest flaws, (2) non-interaction of adjacent flaws and their sparse distribution and (3) sharp Griffith-type microcracks (or flaws). They all are simplifying hypotheses. So, Freudenthal's theory is not a proof of Weibull statistics. Nevertheless, his two-way relationship between material strength and flaws is a valid and useful feature of material failure.

Another problem that challenges the theory of critical flaws is that the Weibull distribution is followed not only by fatigued metals, glasses, ceramics and polymers, in which flaws can be identified in a microscope, but also by concrete at large sizes. However, this material is full of flaws of all sizes, continuously distributed from nano to macro. What is then the largest flaw, and which scale matters? It cannot even be discerned. So why the strength distribution has a Weibull tail?

As proposed in 2005 in [57,59,60], the strength distribution of all non-plastic materials must be anchored on the atomic scale (figure 4). This is the only scale at which the distribution of interatomic bond strength is known exactly. The failure rate of interatomic bonds is governed by random thermal vibrations of atoms (figure 4*d*), whose frequency is $10^{14}\,s^{-1}$. One can estimate that under projectile impact onto concrete in which more than 99.9% of bonds survive, an interatomic bond breaks with the frequency greater than $10^9\,s^{-1}$. So (since $14 - 9 = 5$), even under projectile impact, the atom typically vibrates about 10^5 times before the activation energy barrier is exceeded and the bond breaks. So, even under impact, the thermal vibrations of atoms are always a quasi-stationary process. Therefore, in the process of interatomic bond breaks,

$$\boxed{\text{probability} = \text{frequency}} \tag{3.1}$$

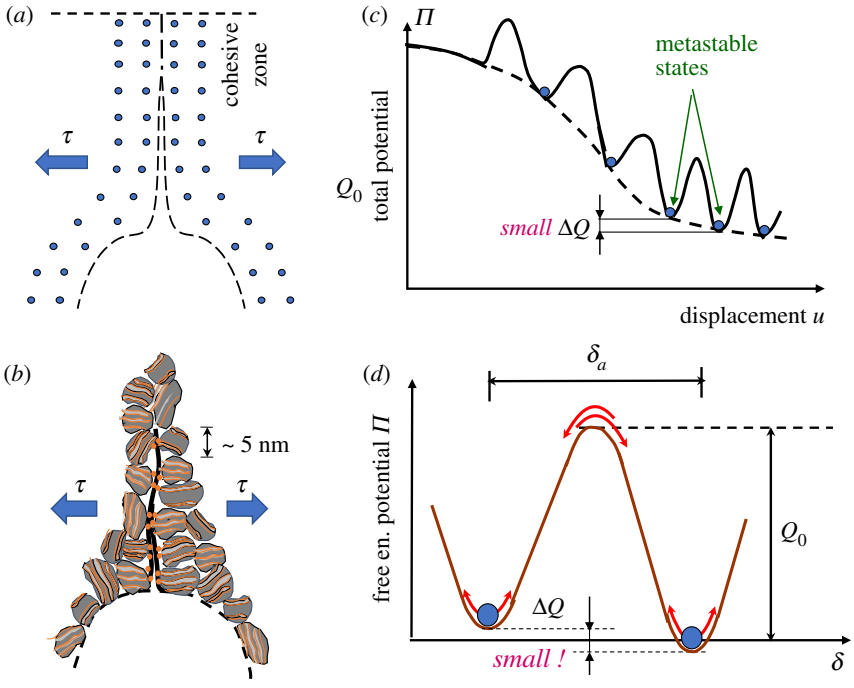

Figure 4. Idealized crack propagating through (*a*) an atomic lattice; and (*b*) a system of nanoglobules (as in hydrated cement). (*c*) Undulations due to atomic crack jumps superposed on a smooth potential energy curve; and (*d*) one potential wave corresponding to crack front jump by one atomic spacing δ_a, showing the activation energy barriers for forward and backward jumps. (Online version in colour.)

(almost the only case where this is not true is the chain reaction in a nuclear bomb). This equality, of course, applies only to the tail of probability distribution, because we deal with rare events.

Imagine a crack propagating through a crystal lattice (or a random system of nanoglobules of cement hydrate), as shown schematically in figure 4*a*,*b*. A pair of atoms does not separate totally right away. Rather, the separation of atoms grows with distance from the tip gradually, by a large number of tiny increments, until the bond in the pair becomes unstable and the crack opens widely. The crack advance by each atomic (or globule) spacing δ_a requires a jump over the activation energy barrier, Q_0 (figure 4*d*). This process superposes onto the descending curve of Π^* of the homogenized lattice an undulating curve (figure 4*c*). Now the important point is that since there are many waves on this curve, each of them corresponding to the front advance by one atomic (or globule) spacing δ_a, the vertical distance between two subsequent valleys on the curve, ΔQ, must be very small (figure 4*c*,*d*).

Thermal excitations of the atoms control the probability of jumps over the activation energy barrier, pictured in figure 4*d*. The activation energy change of these jumps when the crack front advances by one atomic (or globule) spacing δ_a is [29,61–63]:

$$\Delta Q = \delta_a \left[\frac{\partial \Pi^*(c\sigma, a)}{\partial a} \right]_\sigma = \frac{V_a}{E_a} c^2 \sigma^2, \tag{3.2}$$

where σ = macroscopic applied stress; c = nano–macro stress concentration ratio; $c\sigma$ = remote stress applied on the nano-region; E_a = effective elastic modulus of that region; a = crack length; Π^* = complementary energy potential (Gibbs free energy) and V_a = activation volume.

The activation energy barrier for the jumps forward, $Q_0 - \Delta Q/2$ is less than it is for the jumps backward, $Q_0 + \Delta Q/2$, and so, according to Kramers' equation of the transition-rate theory of Boltzmann-type atomistic statistical mechanics [64–67], the net frequency of jumps over the

activation energy barrier is

$$f_a = \nu_T \left(e^{Q_0 - \Delta Q/2/kT} - e^{Q_0 + \Delta Q/2/kT} \right) \approx \frac{\nu_T V_a}{E_a kT} e^{-Q_0/kT} c^2 \sigma^2, \quad \nu_T = \frac{kT}{h}, \tag{3.3}$$

where T = absolute temperature, k = Boltzmann constant and ν_T = characteristic attempt frequency of reversible transitions (h = Planck constant). Here the difference of two exponentials with exponents differing very little has been replaced by sinh and, since the argument of sinh is generally small enough, the sinh has further been be replaced by a linear function of the argument, as shown in equation (3.3) (note that the backward jumps are essential; previously, Zhurkov's theory [68,69] ignored them and yielded an exponential instead of sinh, which overestimated low-stress lifetimes by orders of magnitude [29]).

Since the crack front can jump both forward and backward, the crack tip jumps represent a random walk biased toward forward jumps by the energy release rate. Strictly speaking, this leads to the Fokker–Planck equation governing the place occupation probability of crack tip. However, the Péclet number characterizing this equation is generally so large (greater than 4) that the stress-driven forward jumps of crack tip totally dominate and the random walk aspect is unimportant [29,63].

The second important step is to equate the frequency to probability (equation (3.1)), and to integrate the crack jumps up to the point of instability which is manifested by the wide crack opening (figure 4*a*,*b*). This leads to the essential conclusion that the tail probability of failure on the nanoscale is a power law, and that the exponent is 2 [29,57,59,60]:

$$P_f \propto \sigma^2, \quad C_T = \frac{c \nu_a V_a}{E_a kT} e^{-Q_0/kT} \text{ at tail, for nano} \tag{3.4}$$

This is again true only for the tail of the cumulative probability distribution function (cdf). But nothing more than the tail is needed.

4. Nano–macro scale transition of cdf tails

The question now is how to bridge scales up to the macroscale, that is, over 7 orders of magnitude, from 10^{-8} to 10^{-1} m. Cracks may occur on all these scales. On any given scale, a crack has at its front an FPZ comprising a number of subscale cracks, as shown in figure 4*d*. Along the FPZ, the adjacent cracks are forced to act approximately in parallel coupling, i.e. are constrained to open approximately equally and simultaneously while the forces applied on them are summed. Transversely to the FPZ, the adjacent cracks form a chain, i.e. act approximately in series coupling (figure 5*d*). They are subjected to approximately the same force and their transverse deformations, or openings, are summed. Thus, to make analytical deductions possible, we assume that the transition from one scale to the next involves both parallel and series couplings of elements whose strength follows a cdf which, on the nanoscale, has a power-law tail of exponent 2. The following properties have been proven analytically, for arbitrary postpeak softening behaviour (figure 5*e*) of the coupled elements [57,59,63,70,71]:

(1) In parallel couplings (figure 5*a*), the tail exponents of cdf of the individual elements are additive (which explains why the m of most materials rises in the nano–macro transition from 2 to about 20 to 50).
(2) In series coupling (figure 5*b*), the tail exponent, m, remains unchanged.
(3) Each parallel coupling shortens the reach of the power-law tail by one order of magnitude (while causing convergence to Gaussian cdf in the rest of cdf).
(4) Each 10-fold increase of series coupling extends the reach of power-law tail by one order of magnitude.
(5) The power-law tail of the cdf of strength is indestructible and, while moving up through the scales, its exponent increases, but never decreases.

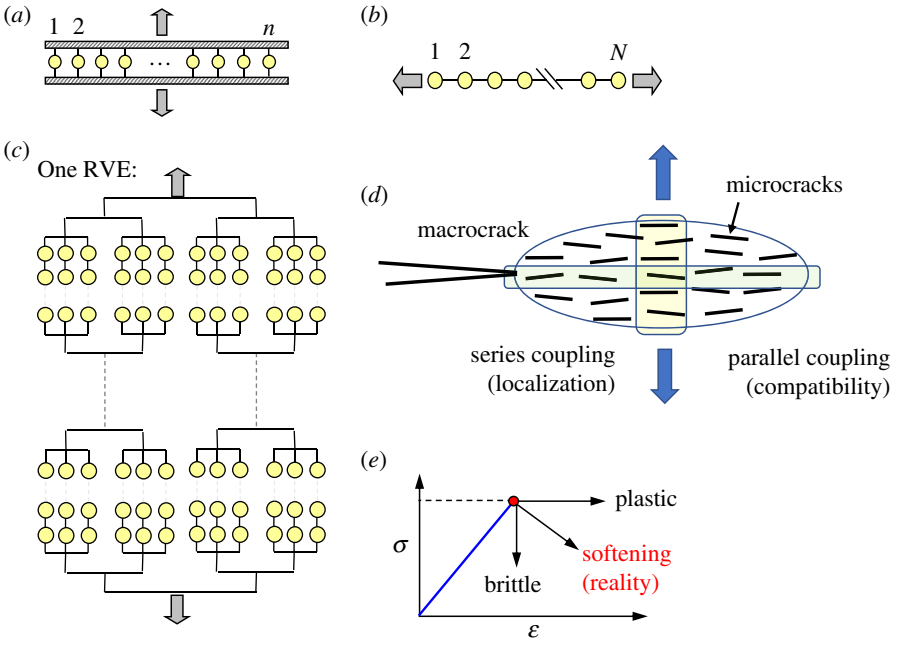

Figure 5. (*a*) Parallel coupling (bundle) and (*b*) series coupling (chain); (*c*) simple hierarchical model combining series and parallel couplings; (*d*) idealized fracture process zone with illustration of microcrack arrays coupled essentially in parallel or in series; (*e*) the stress–strain diagrams of coupled elements considered in calculations. (Online version in colour.)

the special case of property 1 for brittle behaviour was proven by Harlow, Smith *et al.*, Phoenix *et al.* [72,73], and later in a simpler way in [57]) (for time dependence, see [74]).

The foregoing properties can be described by various hierarchical models with parallel and series couplings. A simple one, which gives cdf shapes agreeing (for $P_f > 0.005$) with the tests of concrete and ceramics, is shown in figure 5*c* (another one is the fishnet model, to be discussed later). Refinements such as chain of bundles (2b in figure 2) [75–78] have also been used, but with rather limited experimental or Monte Carlo simulation support.

5. Distribution of structural strength in Type 1 failures and its size dependence

As shown analytically for the cdf tail and demonstrated numerically for the rest of cdf, the hierarchical model in figure 5*c* leads to a graft of Gaussian and Weibull distributions shown, for $N_{eq} = 1$, in figure 6*a*. The (cumulative) failure probability, P_f, is plotted versus material strength σ in the Weibull scale, in which the Weibull distribution is a straight line of a slope equal to Weibull modulus m, and the Gaussian (or normal) distribution deviates from this line to the right while moving to higher P_f.

Now let us focus on Type 1 failure of structures with many RVEs, which is typical of most ceramic parts, unreinforced concrete structures and various rock structures. Since the failure of one RVE triggers dynamic crack propagation leading to overall failure, the structure behaves exactly like a chain, each link corresponding to one RVE (figure 5*b*). The structure size, D, can be measured by the number, N_{eq}, of RVEs in structure, adjusted according to the stress field. For unform tension, $N_{eq} = N$ = the actual number of RVEs in the structure. When the stress is nonuniform, as, e.g. in bending, the RVEs with low stress contribute negligibly to P_f of the structure (e.g. for $m = 24$ and for $\sigma = 75\%$ of σ_{max}, the contribution to the overall P_f is 0.001 compared to the RVE at σ_{max}; for 50%—6×10^{-8}; for 25%—3×10^{-15}).

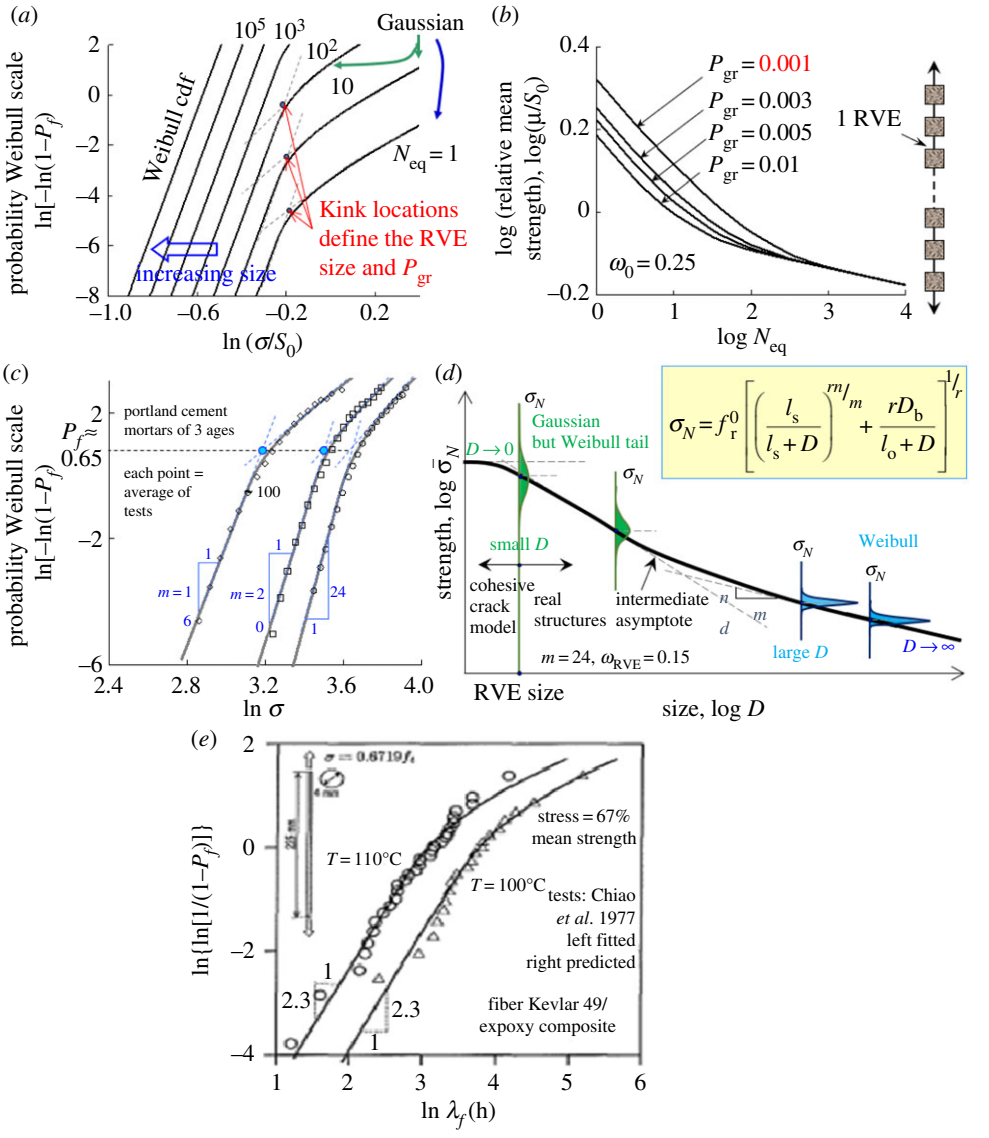

Figure 6. Evolution (in Weibull scale) of structure strength probability distribution with increasing structure size or number of RVEs; (*b*) dependence of size effect on mean nominal strength on the probability at Gauss–Weibull grafting point for one link; (*c*) histograms of the tensile strength of concretes of different ages obtained in Weibull's test [24]; (*d*) Type I energetic-statistical size effect; (*e*) Example of measured [79] and predicted temperature effect. (Online version in colour.)

The chain survives if all the links survive. Consequently, the application of the joint probability theorem yields:

$$P_f = 1 - [1 - P_1(\sigma)]^{N_{eq}}, \tag{5.1}$$

where $P_1(\sigma)$ is the failure probability of one RVE under stress σ (taken as the maximum principal stress if the other principal stresses are perfectly statistically correlated). Because $P_1(\sigma)$ has a power-law tail, $\lim_{N_{eq}\to\infty}$ gives the Weibull distribution, but $N_{eq} \to \infty$ makes sense only if the structure is brittle rather than quasibrittle.

Traditionally, N_{eq} has always been tacitly assumed large enough to consider it as infinite. In that case, and based on the fact that P_1 of each RVE must have a power law tail, σ^m, equation (5.1)

converges to the two-parameter Weibull distribution [24]:

$$P_f = \lim_{N_{eq}\to\infty} \{1 - [1 - P_1(\sigma)]^{N_{eq}}\} = 1 - e^{-(\sigma/s_0)^m}. \tag{5.2}$$

Here m is the Weibull modulus (or shape parameter, which is uniquely related to the coefficient of variation); σ is the stress in the chain; for a structure, σ is proportional to the nominal stress in the structure and s_0 is a scaling parameter depending the stress field, and thus on the geometry of the structure (undergoing Type 1 failure). The asymptotic left tail of Weibull cdf is of the type σ^m.

An important point, which has traditionally been, and still mostly is, ignored, is that, for quasibrittle structures, N_{eq} cannot be considered infinite. Therefore, equation (5.1) must be used instead of the Weibull distribution. It does not give a straight line in Weibull plot (figure 6*a*,*c*).

The finiteness of the weakest-link chain automatically accounts for the fact that the energetic part of Type 1 size effect (figure 1*b*) can be regarded and mathematically derived as the limit case of the energetic size effect when the initial crack of notch tends to be equal to the RVE size (e.g. [34]).

The Weibull–Gaussian transition is, for the hierarchical model in figure 5 rather abrupt (but not for the fishnet model discussed later). This is seen in the plots of equation (5.1) (figure 6*a*,*c*) and is verified by the experimental histograms of strength of the ceramics and concrete. The best and most extensive test data up to now are still the histograms of Weibull [24] published in 1939, shown for concretes of different ages in figure 6*c*, in which the scatter was virtually eliminated by grouping an interval with about 100 tests into each data point. Excellent though the data fit looks, it does not provide a complete experimental validation because the lowest data point in figure 6*c* corresponds to $P_f = 0.007$, which is a long way from 10^{-6}.

Extending the asymptotic curves of Weibull and Gaussian portions, one gets the intersection points (circled in figure 6*a*) at which the Weibull–Gaussian transition is centred. Since the structure behaves as a chain, these points move straight up, by constant distances for each 10-fold increase of N_{eq}. Thus, at increasing structure size, the Weibullian left portion of cdf gradually penetrates into the Gaussian right portion; see figure 6*a* and, in linear scale, figure 7. The Gaussian deviations to the right of Weibull straight line were experimentally demonstrated already in 1939 by Weibull's tests of concretes with various ages (figure 6*c*). Because of the abruptness of the Gauss–Weibull transition, the cdf can be well approximated by a graft of Weibull and Gaussian distributions, as described by eqns 50 and 51 in [57].

Previously, these deviations have been attributed to a finite threshold $\sigma_u > 0$, with $(\sigma - \sigma_u)$ replacing σ in equation (5.1), which is known as the three-parameter Weibull distribution. However, this is fundamentally incorrect—the threshold σ_u is 0 [80]. Tracing the aforementioned deviation backwards, a finite threshold σ_u would imply that activation energy Q_0 in equation (3.3) would have to be replaced by $Q_0 - Q_u$ where $Q_u > 0$, which is impossible.

Note that this impossibility is not negated by the appearance of finite threshold in the tests of residual strength when the statistics of damage caused during a longer sustained pre-load is counted separately [81].

Would the classical Freudenthal's theory of critical microscale flaws fit into the present nanoscale based theory? It would, but would not change it. Xu & Le [58] used level excursion analysis to calculate, in a nonlocal continuum framework, the first passage probability of the random fields (or processes) of material resistance being crossed by the stress field randomized by material flaws. They showed that the nanoscale strength distribution with power-law tail is the physical cause of Weibull tail on the macrocontinuum level, and that the nano–macro transition is not qualitatively altered by the critical flaw statistics.

The location of the grafting point on $P_1(\sigma)$ must be determined experimentally. The best way is to exploit the effect of structure size D (or N_{eq} on the mean structure strength (which has the advantage that only about six tests for each of three or four sizes are needed). The typical size effect curves (of Type 1) are shown in figure 6*b* in a plot of $\log\sigma$ vs. $\log N_{eq}$. The Weibull distribution, which corresponds to a grafting point vanishing at $N_{eq} \to \infty$, is approached asymptotically. It gives a power-law size effect that appears in this plot as a straight line of slope

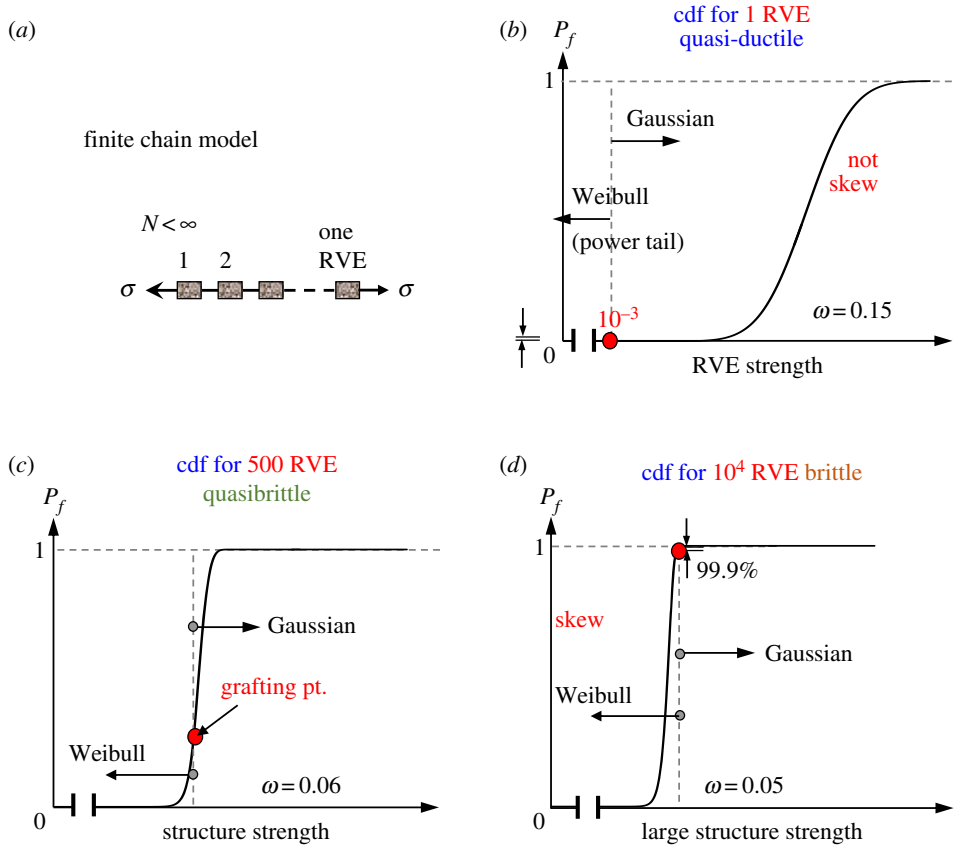

Figure 7. Finite chain modelling Type 1 failure of a structure, and (*b–d*) evolution (in linear scale) of structure strength probability distribution with increasing structure size or number of RVEs. (Online version in colour.)

n/m where n is the number of dimensions of the failure mode (note that even though a beam is three-dimensional one should take $n = 2$ if it is narrow and deep, because mechanics dictates the fracture front to be on one line across the beam width).

Moving in figure 6*b* to smaller D, the mean size effect curve deviates from the Weibull line upwards. A crucial point is that the deviation begins for grafting point probabilities P_{gr} of one RVE at different places. Thus, the size effect tests of mean strength permit identifying the tail grafting probability; for randomly heterogenous quasibrittle materials, $P_{gr} \approx 0.001$ seems universal. Figure 6*b* then implies that the Weibull distribution is followed only by structures so large that $N_{eq} > 10^5$. This is, for example, attained in the overall failure of a large gravity dam. But for all smaller concrete structures, the cdf of strength exhibits the Gauss–Weibull transition.

This analysis also shows that by far the most effective way to calibrate the cdf of material strength is not by testing histograms. Rather, it is by inference from the size effect on the mean strength.

The size effect curves in the form of figure 6b have been verified experimentally for many materials [29,57,63], including concrete [42], limestone [82], fibre composites [83], bone [36,84], etc., and by Monte Carlo simulations [29,63,80] (including those based on the early non-local Weibull theory [85], which works for the mean size effect but not for the tails). An effective finite-element (FE) algorithm for non-local calculation of the P_f of a structure was given in [86].

To sum up, the Type 1 size effect with failure probability distributions may be generally portrayed as shown in figure 6*d*. The figure also shows an accurate asymptotic matching formula for describing the size effect on the mean strength. The horizontal asymptote for $\sigma \to 0$ is

approached only for D smaller than the material inhomogeneities, and thus its usefulness is only theoretical, giving the tail of the size effect curve of the cohesive crack model.

6. Persistence of erroneous assumption of a threshold

Figure 8 shows that the present Gauss–Weibull graft can fit quite well the recently observed experimental histograms of the strength of various tough ceramics [87–90]. However, the experimenters fitted the same histograms by the three-parameter Weibull distributions with a finite threshold (figure 9). Both types of fit seem satisfactory, but it is a misleading illusion, for three reasons:

(1) The slopes m of the lower Weibull portion of the histogram are in figure 8 much higher than in figure 9, which implies a very different size effect (although it was not tested).
(2) If Lohbauer *et al.*'s histogram [88] from figure 8*b* or figure 9*b* is replotted in figure 10*a* as a function of $\log\sigma$, instead of $\log(\sigma-\sigma_u)$, a huge discrepancy in the 10^{-6} tail becomes evident. This implies an enormous error on the unsafe side at the failure probability level that is the maximum tolerable for structural safety.
(3) If Lohbauer *et al.*'s histogram [88] is used to construct the corresponding size effect, with and without thresholds, one gets the curves in figure 10*b*. What is seen is that the histogram fitting by three-parameter Weibull distribution with a finite threshold causes an enormous and dangerous underestimation of the size effect for large sizes (by a factor of 4 for $N_{\mathrm{eq}}=10^9$ RVEs, which is obtained in a cube of side 1000 RVEs under uniform tension).

So, even without knowing the atomistic basis of the failure probability tail, the Weibull distribution with a threshold has been an imprudent choice among two seemingly equivalent possibilities. In favour of the 3-parameter distribution, some testers argue that a specimen loaded to, e.g. 30% of the mean strength never fails. True, but a moot point. For the finite chain or Gauss–Weibull graft, the failure probability would be 0.3^m which, for $m=24$, gives 3×10^{-13}. Considering the test of one specimen to take 20 s, one would have to continue testing as long as the age of the Universe, to be likely to see specimen failure.

7. Lifetime distribution and its size dependence in static and cyclic fatigue

The foregoing theory can be extended to a lifetime under static fatigue (figure 11) and cyclic fatigue. If there is a crack (or notch) to begin with, the first problem is to predict the subcritical crack growth.

This is not a problem of tail probability. Another principle must be used to bridge the scales—nano–macro energy equivalence [29,70,95].

The frequency f_a of ruptures of interatomic bonds provides not only the probability but also the rate of advance, $\dot{a}_n=\mathrm{d}a_n/\mathrm{d}t$, of the nanocrack ($t$ = time, and subscript n labels the nth nanocrack). According to equation (3.3) (in which $\nu_T/kT=1/h=$ constant),

$$\dot{a}_n=\delta_a f_{a_n}=A_n\,\mathrm{e}^{-Q_0/kT}c^2\sigma^2, \tag{7.1}$$

where $A_n=\nu_a V_a/E_a k=\mathrm{const}$. The energy dissipation per unit crack length is $\mathcal{G}\dot{a}$ where $\mathcal{G}$ is the energy release rate per unit crack advance. Now it should be noted that the FPZ of each macrocrack contains many mesoscale cracks, each with its own FPZ that again contains many sub-cracks, each with its own FPZ, and so on (figure 12*b*), all the way to the nanoscale. Energy balance requires that all the energy dissipated per unit time in the FPZ of a macrocrack must be equal to the energy dissipated per unit time by all the nanocracks within that FPZ, i.e.

$$\mathcal{G}\dot{a}=\sum_n \mathcal{G}_n\dot{a}_n. \tag{7.2}$$

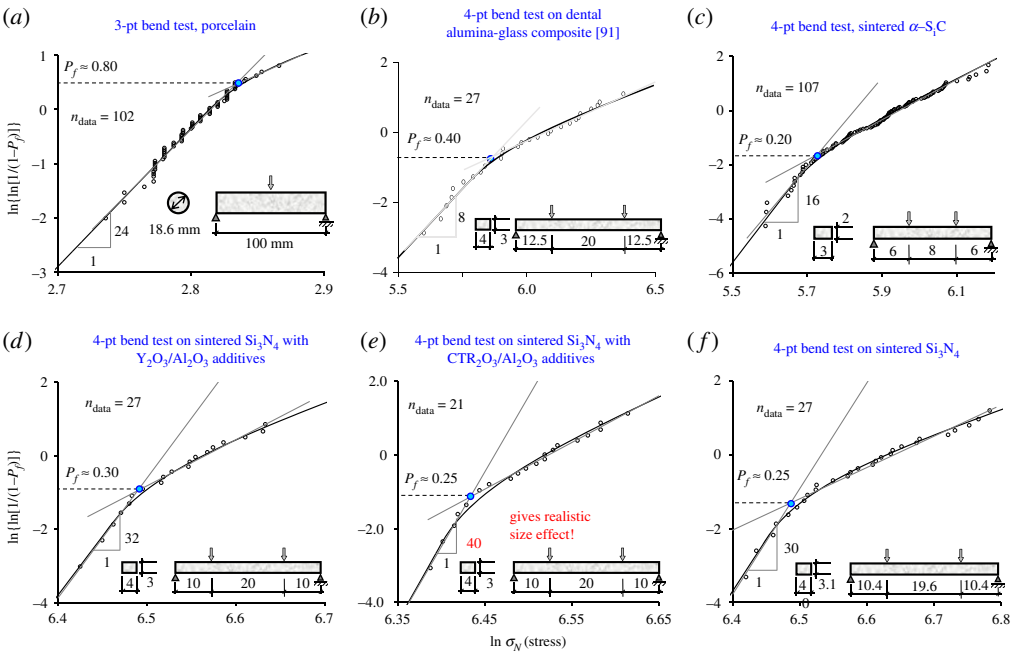

Figure 8. Experimental histograms of tensile strength of various ceramics, compiled from the literature [87–90], optimally fitted by Gauss–Weibull distributions in Weibull scale with zero threshold. (Online version in colour.)

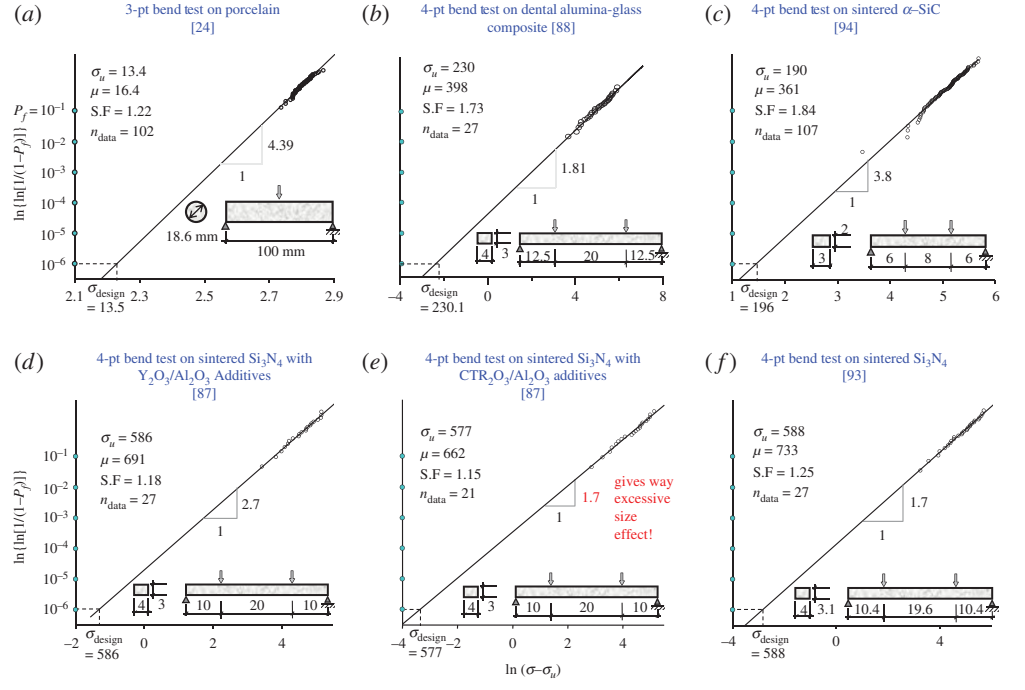

Figure 9. The same histograms as in figure 8 as fitted by the experimenters and presented in three-parameter Weibull scales, each with a different finite threshold. (Online version in colour.)

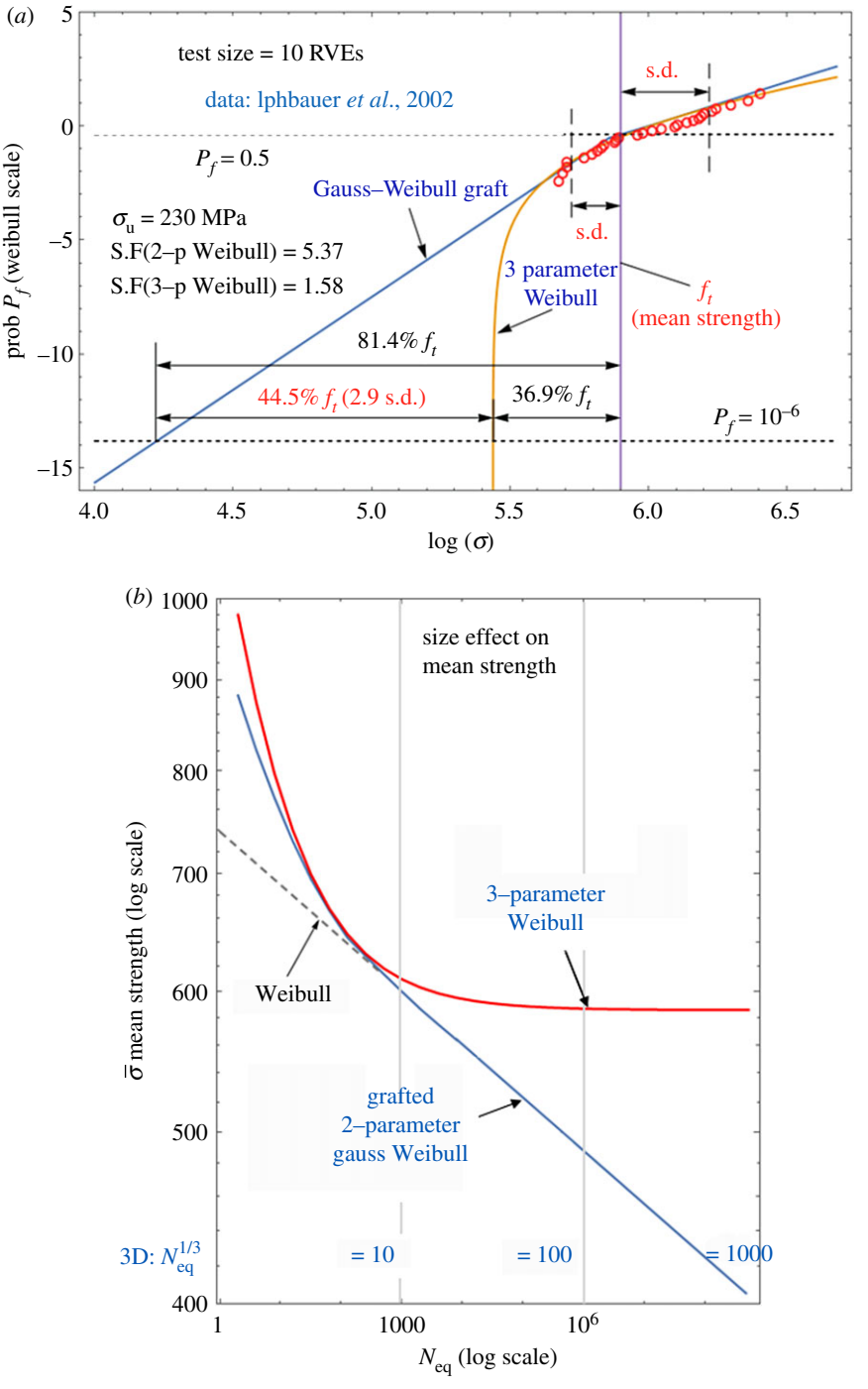

Figure 10. (*a*) Optimum fit of Lohbauer *et al.*'s histogram from figure 9 redrawn in Weibull scale with zero threshold, compared to the Gauss–Weibull fit with zero threshold; (*b*) corresponding size effect curves. (Online version in colour.)

Based on some simplifying approximations, this condition was shown to lead to the macroscale law:

$$\dot{a} = A_s \, \mathrm{e}^{-Q_0/kT} K^n, \tag{7.3}$$

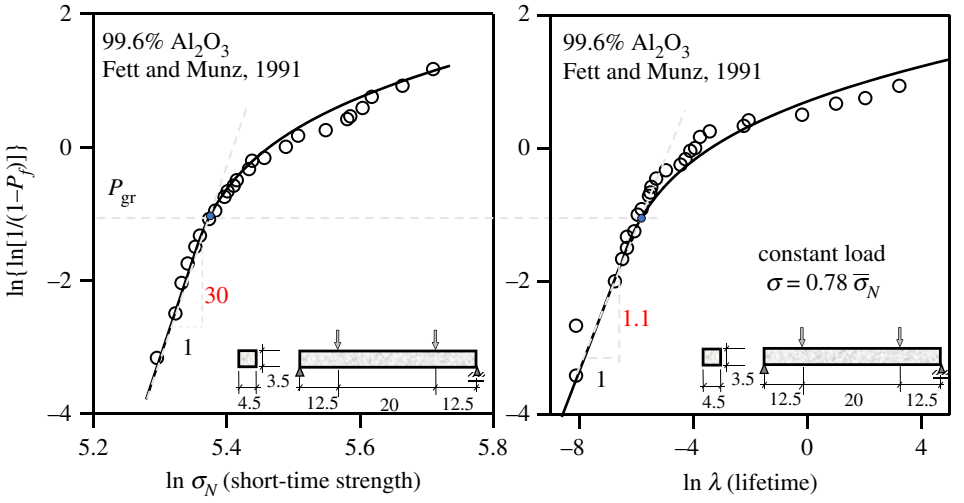

Figure 11. Example of test Fett & Munz's data [92] for short-time strength and lifetime fitted with Gauss–Weibull finite weakest-link chain with the same material parameters. (Online version in colour.)

which is the well-known Charles-Evans law of static subcritical crack growth [97–101] (A_s = constant, K = stress intensity factor). The derivation from energy equivalence shows that the reason for high exponent n is that scale transitions cause n to rise (for concrete, to $n \approx 10$).

The analysis of subcritical crack growth rate under cyclic fatigue is similar, but with one important difference. Regardless of the maximum and minimum of the stress intensity factor, K, the stress cycles within the FPZ, produced by the same $\Delta K = K_{\max} - K_{\min}$, will settle, after a few cycles, due to the hysteresis of damage, on the same constant maxima and minima of the mean stress within the FPZ [102,103]. They are independent of $K_{\max}$ and $K_{\min}$ and depend only on ΔK on the macroscale. Calculation of the crack growth rate again uses the condition of equality of macro- and nanoscale energy dissipations within the FPZ, as written in equation (7.3), but with the difference that the energy dissipation must be integrated over the cycle of stress within the FPZ, varying between the stress maximum and minimum. This calculation [29,70,95] leads to the well-known Paris (or Paris-Erdogan) law [104,105]:

$$\frac{\mathrm{d}a}{\mathrm{d}N} = A_c\, \mathrm{e}^{-Q_0/kT} \Delta K^n, \tag{7.4}$$

established empirically in the 1960s (A_c = constant, N = number of cycles).

If the subcritical static or cyclic growth of the crack leads to a crack of length a not negligible compared to structure size D, of if the crack starts from a long enough notch, the crack growth rate $\mathrm{d}a/\mathrm{d}t$ or $\mathrm{d}a/\mathrm{d}N$ is subjected to the energetic size effect. Due to their large FPZ, this is a typical consequence for concrete and other quasibrittle materials, as confirmed for cyclic fatigue in 1991 by the tests (figure 11*d*) by Bažant & Xu [10,96,106], and recently stronger by Le *et al.* [82] (doubtless the same size effect occurs for all quasibrittle materials when D is not large enough compared to the inhomogeneities, which are of sub-micrometre scale in metals). These and further tests [106] confirmed the size effect generalization of the Paris law, which reads:

$$\frac{\mathrm{d}a}{\mathrm{d}N} = A_c\, \mathrm{e}^{-Q_0/kT} \left(1 + \frac{D_{0c}}{D}\right) \Delta K^n, \tag{7.5}$$

where D_{0c} is the transitional size, a constant. In [96], this constant was assumed to be equal to D_0 for monotonic short-time loading. Recently, though, it was concluded [29] that D_{0c} must be smaller than D_0 (for concrete by about 10%) because the FPZ for cyclic loading is slightly smaller than the FPZ for short-time monotonic loading (as concluded by Rice [102]).

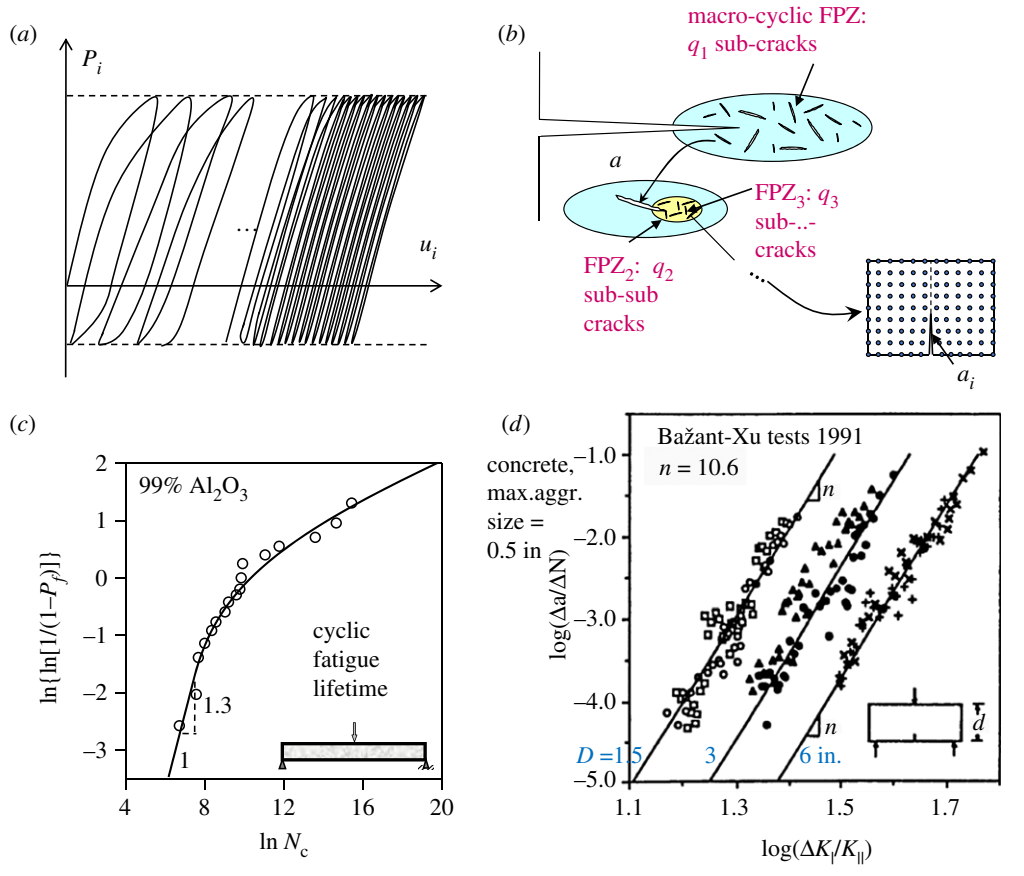

Figure 12. (*a*) Typical cyclic fatigue loading; (*b*) fracture process zones at subsequent scales and cracks in their subscales; Schematic fracture process zone in Mode I fracture; (*c*) Gauss–Weibull fit of cyclic fatigue lifetime data [29]; (*d*) test that revealed in 1991 the size dependence of Paris law in quasibrittle materials [96]. (Online version in colour.)

Here we may digress to note a related viscoelastic property, evident in concrete.

As experimentally identified in [37], the higher the loading rate, the smaller the D_0 value in the SEL [107], equation (1.2). A smaller D_0 means milder brittleness on the Type 2 size effect curve (for this reason, the displacement velocity in size effect testing of concrete should be selected so that specimens of various sizes would reach the maximum load in about the same time).

To analyse the lifetime, consider again structures of positive geometry. The (finite) weakest-link chain model applies to lifetime because the structure fails at the time of first link failure. So the distribution of lifetime for static and well as cyclic fatigue must again follow equation (5.1). As N_{eq} grows with structure size, there is a size effect on the lifetime, which may again be approximated by the Gauss–Weibull graft. A remarkably simple relationship (corroborated by tests of Fett & Munz [92,108,109], figure 11) has been found in [29,70] to obtain the Weibull modulus, $\bar{m}$, for the lifetime under static fatigue loading:

$$\bar{m} = \frac{m}{n+1}, \tag{7.6}$$

where m is the Weibull modulus of the Gauss–Weibull graft for short-time monotonic loading, and n is the exponent of the Charles-Evans law (7.3). Since n is for quasibrittle materials of the order of 10, equation (7.6) shows that the Weibull modulus for lifetime is about an order of magnitude smaller than it is for short-time strength. It also shows that the lifetime distribution can

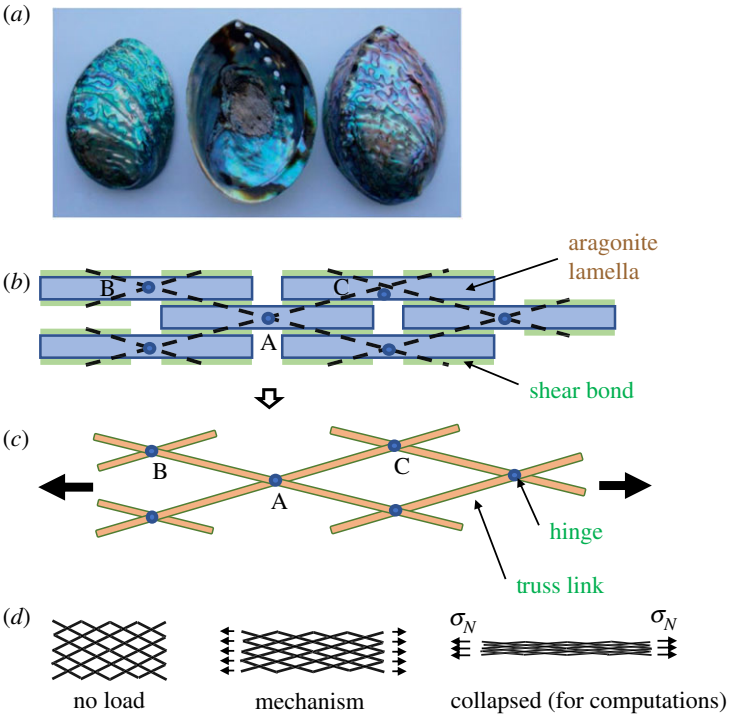

Figure 13. (*a*) Nacre in abalone shell (image courtesy Wikimedia Commons/Doka54); (*b*) schematized imbricated (staggered) lamellar architecture of nacre at sub-micrometer scale; (*c*) fishnet truss capturing the essential force transmission mode; (*d*) rectangular fishnet simulated statistically and its collapsed state used in Monte Carlo simulations. (Online version in colour.)

be predicted by: (1) measuring the size effect on the mean σ_N under short-time monotonic loading, which gives m and (2) testing the crack growth rate for a certain not-too-long time, to get n.

These results greatly simplify predictions of the lifetime. Its distribution can be obtained merely by: (1) measuring the size effect on the mean σ_N under short-time monotonic loading, which gives m, and (2) testing the crack growth rate for a short time, sufficient to get n.

The S–N curve (or Basquin law [110]) for the lifetime of quasibrittle structures without any macrocrack has also been shown to be subjected to size effect ([29,70]).

8. Fishnet distribution for imbricated lamellar materials

Another interesting extension of quasibrittle probabilistic mechanics recently clarified the failure behaviour of nacre and nacreous biomimetic materials. The nacre of pearle oyster or abalone (figure 13*a*) has been known for its amazing strength, an order of magnitude higher than the macroscale strength of its main constituent, the aragonite (a form of $CaCO_3$). Deterministic explanations based on fracture mechanics have been found during the last two decades [111–118]. But, for biomimetic engineering applications, one needs a probabilistic analysis establishing the tail failure probabilities. To this end, a new failure model, called the fishnet model (figure 13*b*,*c*), significantly different from the hierarchical model already described, was discovered in 2017 to reflect the 'brick-and-mortar' architecture of nacre [54–56] and will now be briefly reviewed.

On the sub-micrometre scale, the nacre consists of a lamellar system of overlapping imbricated (or staggered) nanoscale lamellae (or platelets) shown in figure 13*b* and idealized in figure 13*c*. Almost no tension gets transmitted between the ends of two adjacent lamellae, and virtually all the longitudinal load gets transmitted by shear through nanoscale biopolymer layers between bonding lamellae. The links of the lamellae in adjacent rows are imagined as force transmission lines connecting the lamellae centroids (figure 13*b*). The links form a system that looks like a

fishnet pulled diagonally (figure 13*c*,*d*) and can be simulated by a FE program for pin-jointed trusses (in computations, the fishnet is allowed to collapse under horizontal tension into one line, as shown in figure 13*d* (right), because what matters is only the alternating staggered node links).

(a) Brittle fishnet statistics

Consider a rectangular fishnet with k rows and n columns (figure 13*d*), loaded uniformly by uniaxial stress σ imposed at the row ends. The links are assumed to be brittle, i.e. fail suddenly when their stress reaches the random strength limit. Let $P_f(\sigma)$ be the failure probability of fishnet loaded by σ. The failure probability of each link, $P_1(\sigma)$ is assumed to follow the Gauss–Weibull graft with grafting probability determined empirically. Let $P_{S_n}(\sigma)$ with $n = 0, 1, 2, 3, \ldots$ be the survival probabilities of the fishnet when exactly n links have already failed.

Since these are mutually exclusive (disjoint) events the survival probability of the fishnet may be expressed as

$$1 - P_f(\sigma) = P_{S_0}(\sigma) + P_{S_1}(\sigma) + P_{S_2}(\sigma) + \cdots \tag{8.1}$$

Except for unusually low coefficient of variation of link strength, the terms in this sum are normally decreasing rapidly and those with $n > 3$ are normally insignificant.

The first term, $P_{S_0}(\sigma)$, is equivalent to the finite weakest-link model with the Gauss–Weibull distribution. The second term can be calculated according to the theorems of probability of joint and disjoint events and is expressed as

$$P_{S_1}(\sigma) = NP_1(\sigma) \cdot \prod_{i=1}^{N-1} [1 - P_1(\lambda_i \sigma)], \tag{8.2}$$

where λ_i is the stress redistribution factor in the ith link, which is, for simplicity, obtained deterministically, by solving the decay of a disturbance from the Laplace equation that homogenizes the fishnet; λ_i can be greater than or equal to 1 or less than 1 but the shielding zone with less than 1 can be ignored (since it offers almost no chance of link failure). As shown in [54,55], the third term, albeit less simple, can also be calculated analytically, by applying to link failures the theorems of probability of joint and disjoint events while taking into account the stress redistribution within the neighbourhood of previously failed two links.

The results for the cases where 0, 1 or 2 links have already failed are three survival probability distributions whose counterparts, the failure probability distributions, are plotted in Weibull scale in figure 14*a* (for $k = 16$ rows and $n = 32$ columns). The uppermost curve is the straight line of Weibull distribution deviating towards Gaussian on top. The figure also shows, by circle points, the curve obtained by one million Monte Carlo simulations of the fishnet failure (about 10^4 simulations are lumped into each data point, and the points are virtually exact within $P_f > 10^{-5}$; the link strength is assumed to be Gauss–Weibull grafted at $P_f = 0.015$ and its CoV = 7.8%. Note that the curve for the cases with up to two links failed is very close to this exact solution. An analytical expression for the fourth term, $P_{S_3}(\sigma)$, is possible but very complicated and yields little gain. The last computed histogram, with no matching analytical distribution, is the complete solution for any number of links failed.

The terms after the first in equation (8.2), which represent the difference from the finite weakest-link chain, are obviously beneficial for survival. In addition to the to localized transition from the Gaussian curve to the Weibull straight line of slope m occurring at high P_f, there is, while moving to lower P_f, a transition to precisely a doubled slope in figure 14*a* when the second term of equation (8.1) kicks in. At still lower P_f, there is a transition to tripled slope, etc. Thus, the size effect curve can be regarded as an envelope to a sequence of what is called the intermediate asymptotes [119,120], each corresponding to one term in the sum of equation (8.1). With each added term, the intermediate asymptote slope is raised by m (figure 14*a*). Evidently, the nacreous material architecture produces in Weibull scale a progressively steeper dipping curve diverging more and more from the Weibull straight line (figure 14*a*). For many terms, the slope would

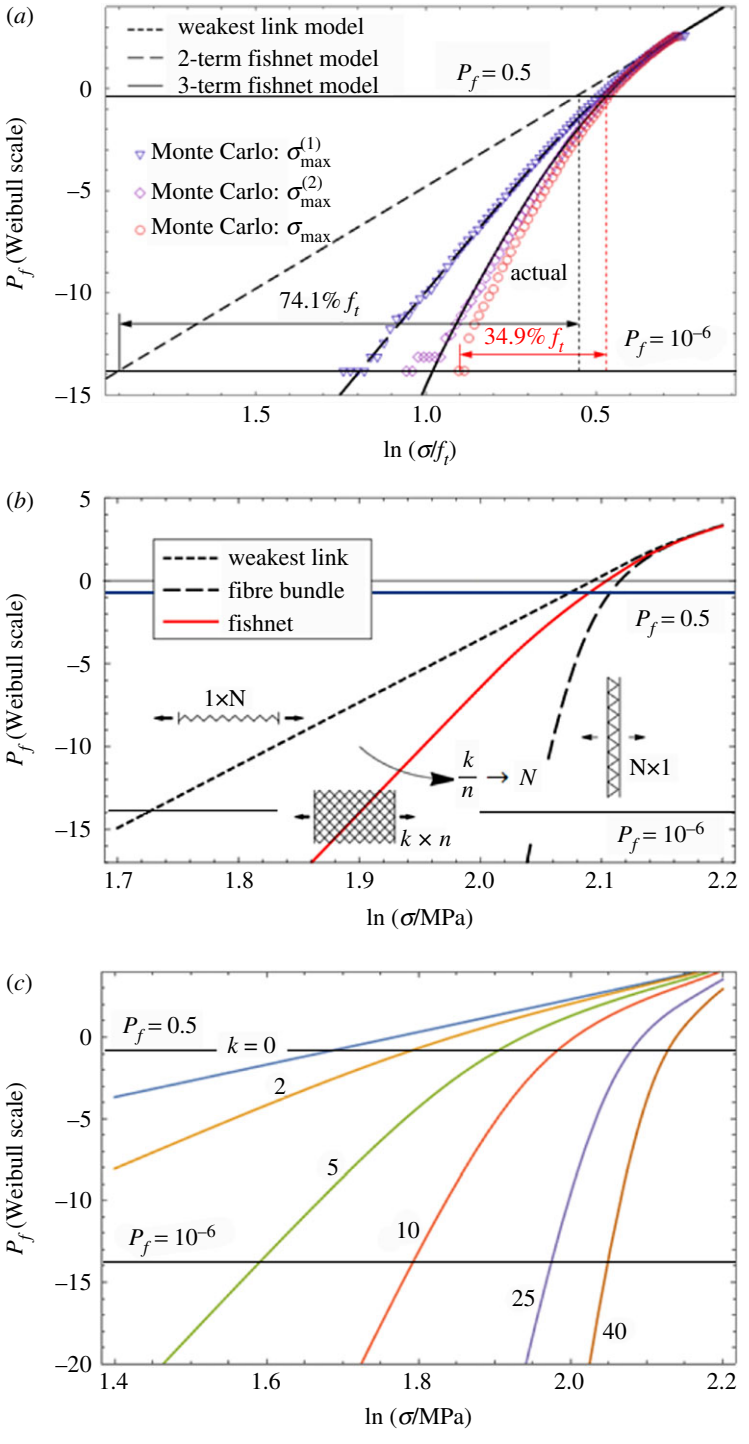

Figure 14. (*a*) Weibull scale plots of two-term and three-term fishnet distributions compared to Gauss–Weibull graft (dashed line) and actual distribution via million Monte Carlo simulations (CoV = 7.8% for each link); (*b*) continuous transition from straight Weibull line (dashed) to Gaussian distribution for pure parallel coupling obtained by changing aspect ratio of fishnet; (*c*) Failure probability distributions for a fishnet with softening links obtain from order statistics (or order 2, 5, 10, etc.). (Online version in colour.)

become nearly vertical but would be practically irrelevant because the corresponding probability would be orders of magnitude below 10^{-6}.

An analytical expression for the fourth term would be possible but rather complicated. However, for more than three terms, the asymptotic slope is approached only at too small a P_f (i.e. for less than or equal to 10^{-6}). So, for the usual coefficient of variation of the link strength, the analytical expressions for the first three terms in equation (8.1) seem to provide a good enough approximation for practice.

When the aspect ratio (or shape) of the fishnet, k/n, changes, the distribution does, too. For $k/n \to 1$, the fishnet cdf converges to the finite weakest-link chain (of Gauss–Weibull cdf) and for $k/n \to \infty$ to the fibre bundle (approaching Gaussian cdf). In this way, the fishnet offers continuous transition between these two basic classical models (figure 2).

So, as we see, in addition to the well-known extraordinary mean strength, the nacreous material architecture has a major additional advantage at the probability tail. Compared to the Weibull straight line of slope m, applicable to ceramics, concrete and other randomly heterogeneous materials, the intersections of the horizontal line $P_f = 10^{-6}$ with the Weibull line and with the line of computed points for the fishnet (figure 14*a*), show the tail strength at 10^{-6} to be increased by 72%. This is an enormous safety advantage of the fishnet material architecture.

Recent studies [54,55] revealed some other noteworthy fishnet features. One is that the cdf of fishnet strength always lies, in Weibull plot, between the curves for the weakest-link chain and the fibre bundle for the same total number and same properties of links. So, these two represent bounds (figure 14*b*).

Also note that the larger the scatter of link strength, the higher the number of links that are likely to fail before reaching the maximum load. This reveals another advantage of fishnet connectivity in the microstructure—for an increasing scatter in link strength (and probably also for increasing scatter in the overlap length of adjacent lamellae), the cumulative probability distribution exhibits, in Weibull plot, an increasingly steeper lower left tail compared to the weakest-link model. Thus, the ratio of the mean failure stress to the stress at the 10^{-6} tail gets decreased, maybe even greatly. Thus, the fishnet scatter may increase structural safety, unless the mean strength gets decreased by scatter even more.

It is no surprise that, under geometric scaling, the mean fishnet strength exhibits a significant size effect. The size effect is similar, though not identical, to Type 1 size effect [29] in quasibrittle random heterogeneous materials. In [29] it is shown that the size effect curve descends in the bilogarithmic plot at continuously decreasing slope. Compared to quasibrittle randomly heterogeneous materials, it is steeper for medium sizes but terminates at large sizes with a lower asymptotic slope. This slope is $1/3m$, rather than $1/m$, for the first three terms of equation (8.1), which tends to mitigate the Type 1 size effect for very large sizes. On the other hand, for the limit case of negligible scatter, the fishnet fails at the first link failure and the finite weakest-link model applies.

(b) Softening fishnet statistics

The foregoing discussion is predicated on assuming the fishnet links to be brittle or almost brittle. However, the shear bond between the adjacent lamellae may exhibit progressive softening, and so may the links. In that case, a different mathematical approach is needed [56], resting on two ideas:

(1) The postpeak softening curve of each link of random strength is approximated by a series of small sudden discrete stress (and stiffness) drops, and
(2) the effect of the drops is treated by the theory of order statistics [121], in which the failure probability is controlled by the link with the kth smallest strength ($k = 1, 2, 3, \ldots$).

In this approach, as it appears, the stress redistributions due to the numerous small drops of strength and stiffness are so feeble that they can be ignored. The analysis leads, for various k, to

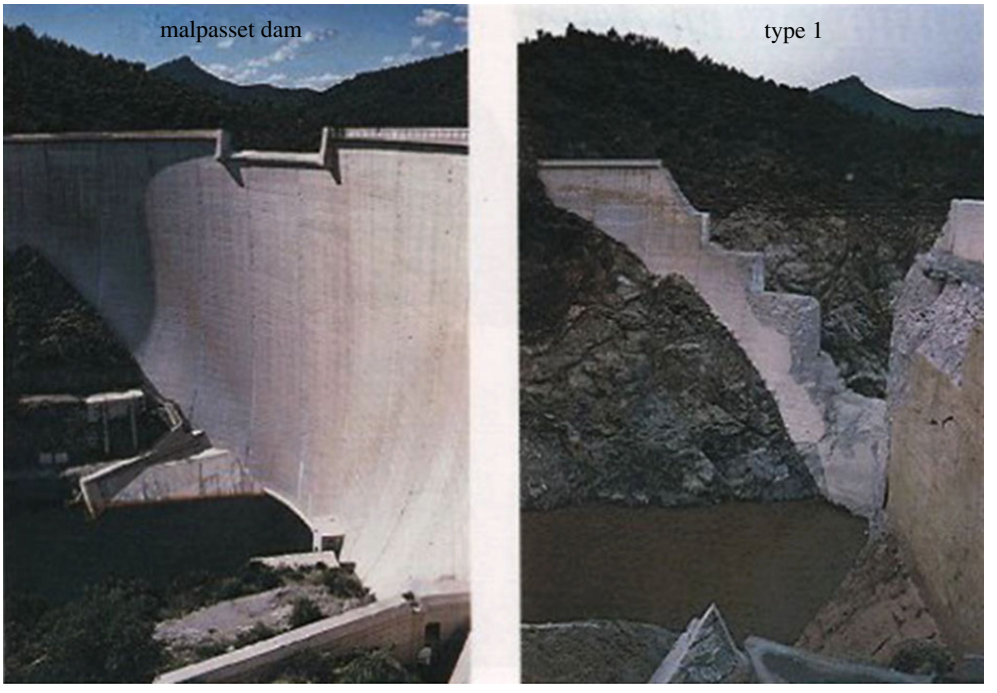

Figure 15. Malpasset Dam before and after failure caused by abutment slip and aggravated by Type 1 size effect. (Online version in colour.)

a series of progressively steepening cdf curves (figure 14*c*). The strength problem is thus reduced to determining which k corresponds to the maximum load [56].

9. Some ramifications and structural engineering applications

The safety design is, in structural engineering, based on the Cornell reliability index and, in a more refined form, on the Hasofer–Lind reliability index. Both can be uniquely linked to the failure probability but have long been based on assuming the structural strength to have a Gaussian distribution. Le [122] recently developed important corrections to these indices, based on the finite weakest-link model and Gauss–Weibull distribution [29, ch. 11].

Another generalization is needed when there is non-negligible, but still not too long, notch or preexisting crack. In that case, there is a more complex continuous transition between the Types 1 and 2 of the statistical-energetic size effect, which has recently been formulated on the basis of asymptotic matching and extensive experiments on concrete [29,43]. Furthermore, the finite weakest-link model has also been extended by J.-L. Le to fracture in V-notches of various angles, and to bimaterial fracture (cf. [29]).

The Weibull distribution has long been used to assess the electronic breakdown probability of dielectrics. Recently, though, for the high-k dielectrics, for which the thickness dropped to 5 nm, major deviations from the Weibull distributions have been observed. The observed deviations were similar as for the finite weakest-link chain for quasibrittle materials. A rigorous mathematical analogy with the electronic breakdown has been identified [123,124], and the theory adapted from strength probability has been shown to describe well the deviations. Further refinement has been presented by J.-L. Le [124].

One problem where the finite weakest-link chain is important is the failure of large plain concrete structures such as dams, retaining walls and footings. A tragic historical disaster, the 1959 failure of Malpasset Dam in French Alps (figure 15), which was the tallest and slenderest

arch dam in the world. The dam failed, at first complete filing, because of excessive slip of schist in the abutment was analysed. The slip led to a vertical crack in the 8 m thick shell of the arch of the dam, and the statistical Type 1 size effect must have come into play. The conclusion from the analysis in [29,125] (improving on [126]) is that the tolerable abutment displacement should have been one half of that considered in design, which was at a time when the size effect was unknown.

In concrete engineering, another statistical problem intervenes. The designer specifies the concrete compression strength, f'_c, which is the only material characteristic used in design codes. The builder then chooses one of many possible concrete mixes, which all can ensure the specified strength, but can lead to great differences in other concrete properties. This uncertainly introduces enormous scatter in the databases, such as the database for shear strength of reinforced concrete beams. Thus, the superposed uncertainty in the choice of concrete, which has nothing to do with mechanics, may significantly modify the strength distribution of the finite weakest-link model. This has been an underappreciated problem. It was discussed in [127] and rigorously analysed in [128], but deeper studies are called for.

10. Main points and final thoughts

(1) The basic simple ideas underlying the quasibrittle failure theory of randomly heterogeneous materials are four:
   (a) The only scale at which the failure probability is known beyond doubt is the atomic scale, at which *frequency* = *probability*, of interatomic bond breaks.
   (b) According to the activation energy theory, the tail of the failure probability distribution at nanoscale must be a power law of stress with exponent 2, and its threshold must be 0.
   (c) In the transition to the material macroscale, the power law is indestructible, its exponent must increase, and the threshold must remain zero.
   (d) The weakest-link chain model for quasibrittle structures must have a finite number of links, each being one RVE that is a potential FPZ. The result is a strength distribution with a size-dependent transition from Weibullian to Gaussian.

(2) Extension to static and cyclic subcritical crack growth, required to predict the distribution of structure lifetime, rests on a fifth idea—mathematical consequence of the necessity of the energy dissipation rates on the macro and nanolevels (figure 12*b*) being equal.

(3) The size effect on the mean structural strength is the most important attribute of failure statistics. Its measurement is essential for validating and calibrating the distributions of structural strength as well as lifetime.

(4) In addition to (i) the weakest-link model, either infinite (Weibull 1939 [24]) or finite [60]), and to (ii) the fibre-bundle model (Daniel [53]), the fishnet is now the third strength probability model tractable analytically (figure 1).

(5) The fishnet statistics inspired by the material architecture of nacre implies a major safety gain at the 10^{-6} strength probability tail and may mitigate the statistical size effect at large sizes. This is intuitively expected since the fishnet architecture provides a transition from the weakest-link towards the fibre-bundle models.

(6) The present demonstration of the widely different shapes of failure probability distribution curves of quasibrittle and nacreous materials accentuates the importance of maximizing in design not the mean strength but the strength at the 10^{-6} tail of failure probability.

(7) Maximization of material strength at the 10^{-6} tail cannot be achieved by histogram testing. The only way is by inference from the tests of size effect on the mean strength, based, inevitably, on a rational and experimentally corroborated theory of the failure probability distribution.

(8) Experimentally, the distribution of strength has never been verified below failure probability 0.005, three and a half orders of magnitudes above the goal (although 80 years

of experience may be seen as a verification of safety for metallic airframes). Thus, e.g. the Gauss–Weibull distribution for concrete, composites and other randomly heterogeneous materials, or the Gaussian distribution for plastic polycrystals, might not be the final answer. The fishnet statistics might play a role for these materials because, in essence, it is an alternative for mingling series and parallel connections in the microstructure, which do not have to take the form of the hierarchical model (figure 5*c*). With a fishnet component, the failure risk at 10^{-6} would be smaller than the pure Gauss–Weibull graft predicts.

(9) Although there exists the stochastic FE method, at present it can hardly provide more statistical information than the coefficient of variation.

(10) In materials science and engineering, it should be realized that designing new materials for superior mean strength may lead to inferior strength at the 10^{-6} probability tail (figure 2*b*), which is what matters for structural safety. *The tail is where the devil is*.

(11) The design of new materials and structures should aim to maximize not the mean strength but the *tail strength*, i.e. the strength at the tail of failure probability less than 10^{-6}. Let it be called the *tail-risk design*—a goal for the future.

(12) The safety factors for structural design, as well as the commercial reliability softwares, ought to be based on the tail risk. In view of the vast computational literature dominated by efforts to improve the fine details of FE algorithms, it is appropriate to conclude this apercu with a caveat:

$$\boxed{|\textbf{Error}| \textbf{ in safety factors} \gg |\textbf{Error}| \textbf{ in FE analysis}} \tag{10.1}$$

Data accessibility. This article has no additional data.

Competing interests. I declare I have no competing interests.

Funding. The work was partially funded under ARO Grant W911NF-19-1-0039 to Northwestern University. Wen Luo, doctoral candidate at Northwestern University, and Jia-Liang Le, associate professor at University of Minnesota, are thanked for their stimulating discussions of the subject.

References

1. Griffith AA. 1921 The phenomena of rupture and flow in solids. *Phil. Trans. R. Soc. Lond. A* **221**, 163–197. (doi:10.1098/rsta.1921.0006)
2. Bažant ZP, Oh B-H. 1983 Crack band theory for fracture of concrete. *Mater. Struct.* **16**, 155–177.
3. Dugdale DS. 1960 Yielding of steel sheets containing slits. *J. Mech. Phys. Solids* **8**, 100–108. (doi:10.1016/0022-5096(60)90013-2)
4. Barenblatt GI. 1959 Formation of equilibrium cracks during brittle fracture: general ideas and hypothesis, axially symmetric cracks (in Russian). *Prikladnaya Matematika i Mekhanika* **23**, 434–444.
5. Barenblatt GI. 1962 Mathematical theory of equilibrium cracks in brittle fracture. *Adv. Appl. Mech.* **7**, 55–129. (doi:10.1016/S0065-2156(08)70121-2)
6. Rice JR. 1968 Mathematical analysis in the mechanics of fracture. In *Fracture—an advanced treatise*, Vol. 2, (ed H Liebowitz), pp. 191–308. New York, NY: Academic Press.
7. Hillerborg A, Modéer M, Peterson PE. 1976 Analysis of crack formation and crack growth in concrete by means of fracture mechanics and finite elements. *Cem. Concr. Res.* **6**, 773–782. (doi:10.1016/0008-8846(76)90007-7)
8. Pijaudier-Cabot G, Bažant ZP. 1987 Nonlocal damage theory. *J. Eng. Mech.* **113**, 1512–1533. (doi:10.1061/(ASCE)0733-9399(1987)113:10(1512))
9. Bažant ZP, Kazemi MT. 1990 Determination of fracture energy, process zone length and brittleness number from size effect, with application to rock and concrete. *Int. J. Fract.* **44**, 111–131. (doi:10.1007/BF00047063)
10. Bažant ZP, Planas J. 1998 *Fracture and size effect in concrete and other quasibrittle materials*. Boca Raton, FL: CRC Press.
11. Bažant ZP. 2005 *Scaling of structural strength*. London, UK: Elsevier.

12. Bažant ZP, Jirásek M. 2002 Nonlocal integral formulations of plasticity and damage: survey of progress. *J. Eng Mech.* **128**, 1119–1149. (doi:10.1061/(ASCE)0733-9399(2002)128:11(1119))
13. Di Luzio G, Cusatis G. 2108 Cohesive crack analysis of size effect for samples with blunt notches and generalized size effect curve for quasi-brittle materials. *Eng. Fract. Mech.* **204**, 15–28. (doi:10.1016/j.engfracmech.2018.09.003)
14. Cusatis G, Bažant ZP, Cedolin L. 2003 Confinement-shear lattice model for concrete damage in tension and compression: II. Computation and validation. *J. Eng. Mech.* **129**, 1449–1458. (doi:10.1061/(ASCE)0733-9399(2003)129:12(1449))
15. Cusatis G, Schauffert E. 2009 Cohesive crack analysis of size effect. *Eng. Fract. Mech.* **76**, 2163–2173. (doi:10.1016/j.engfracmech.2009.06.008)
16. Irwin GR. 1958 Fracture. In *Handbuch der Physik* (ed. Flügge), vol. 6, pp. 551–590. Berlin, Germany: Springer.
17. Bažant ZP. 1976 Instability, ductility, and size effect in strain-softening concrete. *J. Eng. Mech. Div. Am. Soc. Civil Eng.* **102**, 331–344; disc. 103, 357–358, 775–777, 104, 501–502.
18. Bažant ZP, Cedolin L. 1979 Blunt crack band propagation in finite element analysis. *J. Eng. Mech. Div. Proc. ASCE* **105**, 297–315.
19. Bažant ZP, Cedolin L. 1981 *Stability of structures: elastic, inelastic, fracture and damage theories*. Oxford, UK: Oxford University Press.
20. Le JL, Ballarini R, Zhu Z. 2015 Modeling of probabilistic failure of polycrystalline silicon MEMS structures. *J. Am. Ceram. Soc.* **98**, 1685–1697. (doi:10.1111/jace.2015.98.issue-6)
21. Bažant ZP. 2002 Scaling of sea ice fracture—Part I: vertical penetration. *J. Appl. Mech.* **69**, 11–18. (doi:10.1115/1.1429932)
22. Bažant ZP. 2002 Scaling of sea ice fracture—Part II: horizontal load from moving ice. *J. Appl. Mech.* **69**, 19–24. (doi:10.1115/1.1429933)
23. Bažant ZP. 1992 Large-scale thermal bending fracture of sea ice plates. *J. Geophys. Res.* **97**, 17 739–17 751. (doi:10.1029/92JC00816)
24. Weibull W. 1939 The phenomenon of rupture in solids. *Proc. R. Swedish Inst. Eng. Res.* **153**, 1–55. Stockholm.
25. Bažant ZP, Salviato M, Chau Viet T, Viswanathan H, Zubelewicz A. 2014 Why fracking works. *ASME J. Appl. Mech.* **81**, 101010-1–101010-10. (doi:10.1115/1.4028192)
26. Bažant ZP, Li Zhengzhi. 1995 Modulus of rupture: size effect due to fracture initiation in boundary layer. *J. Struct. Eng.* **121**, 739–746. (doi:10.1061/(ASCE)0733-9445(1995)121:4(739))
27. Bažant ZP, Yavari A. 2005 Is the cause of size effect on structural strength fractal or energetic-statistical? *Eng. Fract. Mech.* **72**, 1–31. (doi:10.1016/j.engfracmech.2004.03.004)
28. Bažant ZP, Yavari A. 2007 Response to A. Carpinteri, B. Chiaia, P. Cornetti and S. Puzzi's comments on 'Is the cause of size effect on structural strength fractal or energetic-statistical?'. *Eng. Fract. Mech.* **74**, 2897–2910. (doi:10.1016/j.engfracmech.2007.02.026)
29. Bažant ZP, Le Jia-Liang. 2017 *Probabilistic mechanics of quasibrittle structures: strength, lifetime, and size effect*. Cambridge, UK: Cambridge University Press.
30. Bažant ZP. 1984 Size effect in blunt fracture: concrete, rock, metal. *J. Eng. Mech.* **110**, 518–535. (doi:10.1061/(ASCE)0733-9399(1984)110:4(518))
31. Grassl P, Bažant ZP. 2009 Random lattice-particle simulation of statistical size effect in quasi-brittle structures failing at crack initiation. *J. Eng. Mech.* **135**, 85–92. (doi:10.1061/(ASCE)0733-9399(2009)135:2(85))
32. Chau VT, Bažant ZP, Su Y. 2016 Growth model for large branched 3D hydraulic crack system in gas or oil shale. *Phil. Trans. R. Soc. A* **374**, 20150418. (doi:10.1098/rsta.2015.0418)
33. Rahimi-Aghdam S *et al.* 2019 Branching of hydraulic cracks enabling permeability of gas or oil shale with closed natural fractures. *Proc. Natl Acad. Sci. USA* **116**, 1532–1537. (doi:10.1073/pnas.1818529116)
34. Bažant ZP. 2004 Scaling theory of quaisbrittle structural failure. *Proc. Natl Acad. Sci. USA* **101**, 13 397–13 399. (doi:10.1073/pnas.0405856101)
35. Bažant ZP. 1997 Scaling of quasibrittle fracture: asymptotic analysis. *Int. J. Fract.* **83**, 19–40. (doi:10.1023/A:1007387823522)
36. Bažant ZP, Kim K-T, Yu Q. 2013 Non-uniqueness of cohesive-crack stress-separation law of human and bovine bones and remedy by size effect tests. *Int. J. Fract.* **181**, 67–81. (doi:10.1007/s10704-013-9821-8)
37. Bažant ZP, Pfeiffer PA. 1987 Determination of fracture energy from size effect and brittleness number. *ACI Mater. J.* **84**, 463–480.

38. Bažant ZP, Kazemi MT. 1990 Determination of fracture energy, process zone length and brittleness number from size effect, with application to rock and concrete. *Int. J. Fract.* **44**, 111–131. (doi:10.1007/BF00047063)
39. Christensen RM. 2013 *The theory of materials failure*. Oxford, UK: Oxford University Press.
40. Yasui M, Schulson EM, Renshaw CE. 2017 Experimental studies in mechanical properties and ductile-to-brittle transition of ice-silica mixtures: Young's modulus, compressive strength and fracture toughness. *J. Geophys. Res.* **122**, 6014–6030. (doi:10.1002/2017JB014029)
41. Bažant ZP, Li Z. 1995 Modulus of rupture: size effect due to fracture initiation in boundary layer. *J. Struct. Eng.* **121**, 739–746. (doi:10.1061/(ASCE)0733-9445(1995)121:4(739))
42. Bažant ZP, Novák D. 2000 Energetic-statistical size effect in quasibrittle failure at crack initiation. *ACI Mater. J.* **97**, 381–392.
43. Hoover CG, Bažant ZP. 2014 Cohesive crack, size effect, crack band and work-of-fracture models compared to comprehensive concrete fracture tests. *Int. J. Fract.* **187**, 133–143. (doi:10.1007/s10704-013-9926-0)
44. Freudenthal AM. 1968 Statistical approach to brittle fracture. In *Fracture: an advanced treatise* (ed H Liebowitz), vol. 2, pp. 591–619. New York, NY: Academic Press.
45. Ang AH-S, Tang WH. 1984 *Probability concepts in engineering planning and design. Vol II. Decision, risk and reliability*. New York, NY: J. Wiley.
46. Haldar A, Mahadevan S. 2000 *Probability, reliability, and statistical methods in engineering design*. New York, NY: Wiley.
47. Duckett K. 2005 Risk analysis and the acceptable probability of failure. *Struct. Eng.* **83**, 25–26.
48. Melchers RE. 1987 *Structural reliability, analysis & prediction*. New York, NY: Wiley.
49. NKB. 1978 (Nordic Committee for Building Structures). *Recommendation for loading and safety regulations for structural design*. NKB Report, No. 36.
50. Fisher RA, Tippett LHC. 1928 Limiting forms of the frequency distribution of the largest or smallest member of a sample. *Math. Proc. Cambridge Philos. Soc.* **24**, 180–190. (doi:10.1017/S0305004100015681)
51. Gumbel EJ. 1958 *Statistics of extremes*. New York, NY: Columbia University Press.
52. Bažant ZP. 2001 Probabilistic modeling of quasibrittle fracture and size effect. *Structural safety and reliability* (eds RB Corotis, GI Schueller, M Shinozuka), *Proc. 8th Int. Conf., ICOSSAR, Newport Beach, CA*, pp. 1–23. Swets & Zeitinger (Balkema).
53. Daniels HE. 1945 The statistical theory of the strength of bundles and threads. *Proc. R. Soc. Lond. A* **183**, 405–435. (doi:10.1098/rspa.1945.0011)
54. Luo Wen, Bažant ZP. 2017 Fishnet model for failure probability tail of nacre-like imbricated lamellar materials. *Proc. Natl Acad. Sci. USA* **114**, 12 900–12 905. (doi:10.1073/pnas.1714103114)
55. Luo Wen, Bažant ZP. 2017 Fishnet statistics for probabilistic strength and scaling of nacreous imbricated lamellar materials. *J. Mech. Phys. Solids* **109**, 264–287 (update of Arxiv1706.01591, June 4, 2017). (doi:10.1016/j.jmps.2017.07.023)
56. Luo W, Bažant ZP. 2018 Fishnet model with order statistics for tail probability of failure of nacreous biomimetic materials with softening interlaminar links. *J. Mech. Phys. Solids* **121**, 281–295. (doi:10.1016/j.jmps.2018.07.023)
57. Bažant ZP, Pang S-D. 2007 Activation energy based extreme value statistics and size effect in brittle and quasibrittle fracture. *J. Mech. Phys. Solids* **55**, 91–134. (doi:10.1016/j.jmps.2006.05.007)
58. Xu Z, Le J-L. 2018 On power-law tail distribution of strength statistics of brittle and quasibrittle structures. *Eng. Fract. Mech.* **197**, 80–91. (doi:10.1016/j.engfracmech.2018.04.009)
59. Bažant ZP, Pang S-D. 2005 Revision of reliability concepts for quasibrittle structures and size effect on probability distribution of structural strength. In *Proc. of 9th Int. Conf. on Structural Safety and Reliability (ICOSSAR), Rome* (eds G Augusti, GI Schuëller, M Ciampoli), pp. 377–386. Rotterdam, The Netherlands: MilPress.
60. Bažant ZP, Pang S-D. 2006 Mechanics based statistics of failure risk of quasibrittle structures and size effect on safety factors. *Proc. Natl Acad. Sci. USA* **103**, 9434–9439. (doi:10.1073/pnas.0602684103)
61. Bažant ZP, Le J-L, Bazant MZ. 2008 Size effect on strength and lifetime distribution of quasibrittle structures implied by interatomic bond break activation. In *Proc. of 17th European Conf. on Fracture, Brno, Czech Republic*, pp. 78–92.

62. Bažant ZP, Le J-L, Bazant MZ. 2009 Scaling of strength and lifetime probability distributions of quasibrittle structures based on atomistic fracture mechanics. *Proc. Natl Acad. Sci. USA* **106**, 11 484–11 489. (doi:10.1073/pnas.0904797106)
63. Le JL, Bažant ZP, Bazant MZ. 2011 Unified nano-mechanics based probabilistic theory of quasibrittle and brittle structures: I. Strength, static crack growth, lifetime and scaling. *J. Mech. Phys. Solids* **59**, 1291–1321. (doi:10.1016/j.jmps.2011.03.002)
64. Kramers HA. 1941 Brownian motion in a field of force and the diffusion model of chemical reaction. *Physica* **7**, 284–304. (doi:10.1016/S0031-8914(40)90098-2)
65. Krausz AS, Krausz K. 1988 *Fracture kinetics of crack growth*. Dordrecht, The Netherlands: Kluwer Academic Publisher.
66. Glasstone S, Laidler KJ, Eyring H. 1941 *The theory of rate processes*. New York, NY: McGraw-Hill.
67. Eyring H. 1936 Viscosity, plasticity, and diffusion as examples of absolute reaction rates. *J. Chem. Phys.* **4**, 283–291. (doi:10.1063/1.1749836)
68. Zhurkov SN. 1965 Kinetic concept of the strength of solids. *Int. J. Fract. Mech.* **1**, 311–323.
69. Zhurkov SN, Korsukov VE. 1974 Atomic mechanism of fracture of solid polymer. *J. Polym. Sci.* **12**, 385–398.
70. Bažant ZP, Le J-L. 2009 Nano-mechanics based modeling of lifetime distribution of quasibrittle structures. *J. Eng. Fail. Anal.* **16**, 2521–2529. (doi:10.1016/j.engfailanal.2009.04.019)
71. Salviato M, Bažant ZP. 2014 The asymptotic stochastic strength of bundles of elements exhibiting general stress-strain laws. *Probab. Eng. Mech.* **36**, 1–7. (doi:10.1016/j.probengmech.2014.01.001)
72. Harlow DG, Smith RL, Taylor HM. 1983 Lower tail analysis of the distribution of the strength of load-sharing systems. *J. Appl. Prob.* **20**, 358–367. (doi:10.2307/3213808)
73. Phoenix SL, Ibnanbdeljalil M, Hui C-Y. 1993 Size effect on the distribution for strength of brittle matrix fibrous composites. *Int. J. Solids Struct.* **34**, 545–568. (doi:10.1016/S0020-7683(96)00034-0)
74. Coleman BD. 1958 Statitics and time dependence of mechanical breakdown in fibers. *J. Appl. Phys.* **29**, 968–983. (doi:10.1063/1.1723343)
75. Harlow DG, Phoenix SL. 1978 The chain-of-bundles probability model for the strength of fibrous materials I: analysis and conjectures. *J. Compos. Mater.* **12**, 195–214. (doi:10.1177/002199837801200207)
76. Harlow DG, Phoenix SL. 1978 The chain-of-bundles probability model for the strength of fibrous materials II: a numerical study of convergence. *J. Compos. Mater.* **12**, 314–334. (doi:10.1177/002199837801200308)
77. Harlow DG, Phoenix SL. 1979 Bounds on the probability of failure of composite materials. *Int. J. Frac.* **15**, 312–336.
78. Phoenix SL. 1978 Stochastic strength and fatigue of fiber bundles. *Int. J. Fract.* **14**, 327–344.
79. Chiao CC, Sherry RJ, Hetherington NW. 1977 Experimental verification of an accelerated test for predicting the lifetime of organic fiber composites. *J. Comp. Mater.* **11**, 79–91. (doi:10.1177/002199837701100109)
80. Pang S-D, Bažant ZP, Le J-L. 2008 Statistics of strength of ceramics: finite weakest-link model and necessity of zero threshold. *Int. J. Fract.* **154**, 131–145. (doi:10.1007/s10704-009-9317-8)
81. Salviato M, Kirane K, Bažant ZP. 2014 Statistical distribution and size effect of residual strength of quasibrittle materials after a period of constant load. *J. Mech. Phys. Solids* **64**, 440–454. (doi:10.1016/j.jmps.2013.12.005)
82. Le Jia-Liang, Manning J, Labuz J. 2014 Scaling of fatigue crack growth in rock. *Int. J. Rock Mech. Mining Sci.* **72**, 71–79. (doi:10.1016/j.ijrmms.2014.08.015)
83. Bažant ZP, Zhou Y, Novák D, Daniel IM. 2004 Size effect on flexural strength of fiber-composite laminate. *J. Eng. Mater. Tech. ASME* **126**, 29–37. (doi:10.1115/1.1631031)
84. Bažant ZP, Kim JJH, Daniel IM, Becq-Giraudon E, Zi G. 1999 Size effect on compression strength of fiber composites failing by kink band propagation. *Int. J. Fract.* **95**, 103–141. (doi:10.1023/A:1018640015465)
85. Bažant ZP, Xi Y. 1991 Statistical size effect in quasi-brittle structures: II. Nonlocal theory. *J. Eng. Mech.* **117**, 2623–2640. (doi:10.1061/(ASCE)0733-9399(1991)117:11(2623))
86. Bažant ZP, Le J-L, Hoover CG. 2010 Nonlocal boundary layer (NBL) model: overcoming boundary condition problems in strength statistics and fracture analysis of quasibrittle

materials. In *Proc. FraMCoS-7, 7th Int. Conf. Jeju, Korea* (ed. B-H Oh), pp. 135–143. Seoul, Korea: Korea Concrete Institute.
87. Santos CD, Strecker K, Piorino Neto F, Moreira de Macedo Silva O, Aparecido Baldacum S, Roberto Moreira da Silva C. 2003 Evaluation of the reliability of Si_3N_4-Al_2O_3 -CTR_2O_3 ceramics through Weibull analysis. *Mater. Res.* **6**, 463–467. (doi:10.1590/S1516-14392003000400006)
88. Lohbauer U, Petchelt A, Greil P. 2002 Lifetime prediction of CAD/CAM dental ceramics. *J. Biomed. Mater. Res.* **63**, 780–785. (doi:10.1002/(ISSN)1097-4636)
89. Gross B. 1996 Least squares best fit method for the three parameter Weibull distribution: analysis of tensile and bend specimens with volume or surface flaw failure. *NASA*, TM-4721, pp. 1–21.
90. Duffy SF, Powers LM, Starlinger A. 1993 Reliability analysis of structural ceramic components using a three-parameter Weibull distribution. *J. Eng. Gas Turbines Power* **115**, 109–116. (doi:10.1115/1.2906664)
91. Le JL, Bažant ZP. 2009 Finite weakest-link model with zero threshold for strength distribution of dental restorative ceramics. *Dent. Mater.* **25**, 641–648. (doi:10.1016/j.dental.2008.11.011)
92. Fett T, Munz D. 1991 Static and cyclic fatigue of ceramic materials. *Ceramics today – tomorrow's ceramics* (ed. P Vincenzini), pp. 1827–1835. Elsevier Science Publisher B. V.
93. Gross B. 1996 Least squares best fit method for the three parameter Weibull distribution: analysis of tensile and bend specimens with volume and surface flaw failure. NASA Technical Report TM-4721, pp. 1–21.
94. Salem JA, Nemeth NN, Powers LP, Choi SR. 1996 Reliability analysis of axially ground brittle materials. *J. Eng. Gas Turbines & Power* **118**, 863–871. (doi:10.1115/1.2817007)
95. Le JL, Bažant ZP. 2011 Unified nano-mechanics based probabilistic theory of quasibrittle and brittle structures: II. Fatigue crack growth, lifetime and scaling. *J. Mech. Phys. Solids* **59**, 1322–1337. (doi:10.1016/j.jmps.2011.03.007)
96. Bažant ZP, Xu K. 1991 Size effect in fatigue fracture of concrete. *ACI Mater. J.* **88**, 390–399.
97. Charles RJ. 1958 Static fatigue of glass I. *J. Appl. Phys.* **29**, 1549–1553. (doi:10.1063/1.1722991)
98. Charles RJ. 1958 Static fatigue of glass II. *J. Appl. Phys.* **29**, 1554–1560. (doi:10.1063/1.1722992)
99. Evans AG. 1972 A method for evaluating the time-dependent failure characteristics of brittle materials – and its application to polycrystalline alumina. *J. Mater. Sci.* **7**, 1173–1146. (doi:10.1007/BF00550196)
100. Thouless MD, Hsueh CH, Evans AG. 1983 A damage model of creep crack growth in polycrystals. *Acta Metall.* **31**, 1675–1687. (doi:10.1016/0001-6160(83)90166-9)
101. Evans AG, Fu Y. 1984 The mechanical behavior of alumina. In *Fracture in ceramic materials*, pp. 56–88. Park Ridge, NJ: Noyes Publications.
102. Rice JR. 1967 Mechanics of crack tip deformation and extension by fatigue. *Fatigue crack propagation*. Special Techn. Publ., vol. 415, pp. 247–309. Philadelphia, PA: ASTM.
103. Kirane K, Bažant ZP. 2015 Enhanced microplane model for sub-critical crack growth and size effect under cyclic loading in isotropic quasibrittle solids. *Int. J. Fatigue* **70**, 93–105. (doi:10.1016/j.ijfatigue.2014.08.012)
104. Paris PC, Erdogan F. 1963 A critical analysis of crack propagation law. *J. Basic Eng.* **85**, 528–534. (doi:10.1115/1.3656900)
105. Suresh S. 1991 *Fatigue of materials*. Cambridge, UK: Cambridge University Press.
106. Bazant ZP, Schell WF. 1993 Fatigue fracture of high-strength concrete and size effect. *ACI Mater. J.* **90**, 472–478.
107. Bažant ZP, Gettu R. 1992 Rate effects and load relaxation: static fracture of concrete. *ACI Mater. J.* **89**, 456–468.
108. Fett T. 1991 A fracture-mechanical theory of subcritical crack growth in ceramics. *Int. J. Frac.* **54**, 117–130. (doi:10.1007/BF00028914)
109. Munz D, Fett T. 1999 *Ceramics: mechanical properties, failure behavior, materials selection*. Berlin, Germany: Springer.
110. Basquin OH. 1910 The exponential law of endurance tests. *Proc. ASTEA* **10**, 625–630.
111. Wang RZ, Suo Z, Evans AG, Yao N, Aksay IA. 2001 Deformation mechanisms in nacre. *J. Mater. Res.* **16**, 2485–2493. (doi:10.1557/JMR.2001.0340)
112. Gao H, Ji B, Jäger IL, Arzt E, Fratzl P. 2003 Materials become insensitive to flaws at nanoscale: lessons from nature. *Proc. Natl Acad. Sci. USA* **100**, 5597–5600. (doi:10.1073/pnas.0631609100)

113. Shao Y, Zhao HP, Feng XQ, Gao H. 2012 Discontinuous crack-bridging model for fracture toughness analysis of nacre. *J. Mech. Phys. Solids* **60**, 1400–1419. (doi:10.1016/j.jmps.2012.04.011)
114. Chen L, Ballarini R, Kahn H, Heuer AH. 2007 A bioinspired micro-composite structure. *J. Mater. Res.* **22**, 124–131. (doi:10.1557/jmr.2007.0016)
115. Askarinejad S, Rahbar N. 2015 Toughening mechanisms in bioinspired multilayered materials. *J. R. Soc. Interface* **12**, 20140855. (doi:10.1098/rsif.2014.0855)
116. Dutta A, Tekalur SA, Miklavcic M. 2013 Optimal overlap length in staggered architecture composites under dynamic loading conditions. *J. Mech. Phys. Solids* **61**, 145–160. (doi:10.1016/j.jmps.2012.08.005)
117. Dutta A, Tekalur SA. 2014 Crack tortuousity in the nacreous layer – topological dependence and biomimetic design guideline. *Int. J. Solids Struct.* **51**, 325335. (doi:10.1016/j.ijsolstr.2013.10.006)
118. Wei X, Filleter T, Espinosa HD. 2015 Statistical shear lag model: unraveling the size effect in hierarchical composites. *Acta Biomater.* **18**, 206–212. (doi:10.1016/j.actbio.2015.01.040)
119. Barenblatt GI. 1978 *Similarity, self-similarity and intermediate asymptotics* (in Russian). Moscow, Russia: Girometeoizdat, and English translation, Consultants Bureau, New York 1979.
120. Barenblatt GI. 2003 *Scaling*. Cambridge, UK: Cambridge University Press.
121. Leadbetter MR, Lindgren G, Rootzaen H. 2012 *Extremes and related properties of random sequences and processes*. Springer Science & Business Media.
122. Le J-L. 2015 Size effect on reliability indices and safety factors of quasibrittle structures. *Struct. Saf.* **52**, 20–28. (doi:10.1016/j.strusafe.2014.07.002)
123. Le JL, Bažant ZP, Bazant MZ. 2009 Lifetime of high-*k* gate dielectrics and analogy with strength of quasi-brittle structures. *J. Appl. Phys.* **106**, 104119. (doi:10.1063/1.3256225)
124. Le J-L. 2012 A finite weakest-link model and lifetime distribution of high-k gate dielectrics under unipolar AC voltage stress. *Microelectron. Rehabil.* **52**, 100–106. (doi:10.1016/j.microrel.2011.09.010)
125. Le J-L, Bažant ZP. 2012 Computation of probability distribution of strength of quasibrittle structures failing at macrocrack initiation. *J. Eng. Mech.* **138**, 888–899. (doi:10.1061/(ASCE)EM.1943-7889.0000396)
126. Bažant ZP, Vořechovský M., Novák D. 2007 Asymptotic prediction of energetic-statistical size effect from deterministic finite element solutions. *J. Eng. Mech.* **128**, 153–162. (doi:10.1061/(ASCE)0733-9399(2007)133:2(153))
127. Bažant ZP, Yu Q. 2008 Minimizing statistical bias to identify size effect from beam shear database. *ACI Struct. J.* **105**, 685–691.
128. Le JL, Bažant ZP. 2018 Failure probability of concrete specimens of uncertain mean strength in large database. (http://arxiv.org/abs/2383101).